iScience

Article

Molecular details and phosphoregulation of the CENP-T-Mis12 complex interaction during mitosis in DT40 cells

Graphical abstract

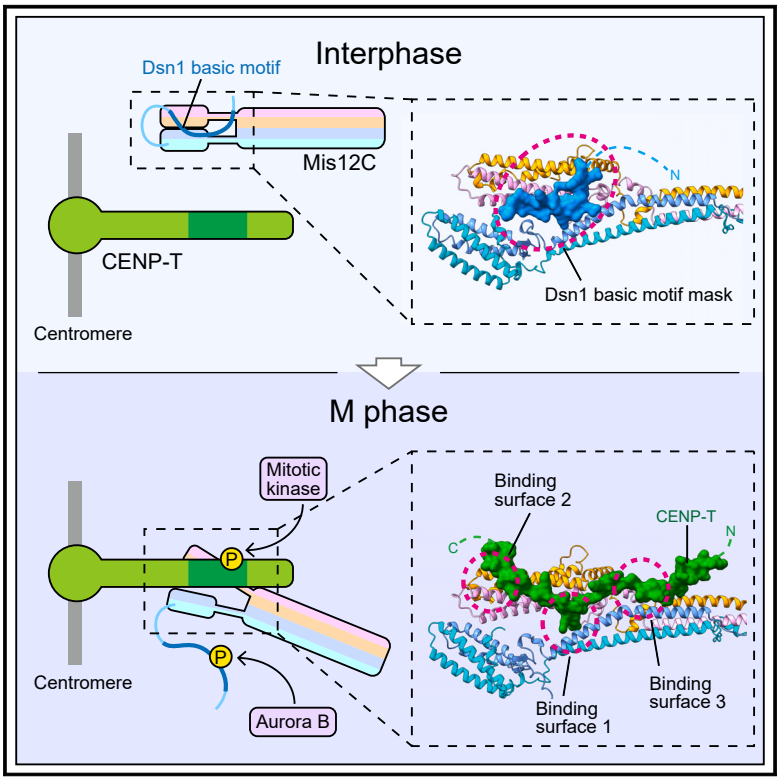

Highlights

- Mis12C interacts with CENP-T only in mitosis
- Three binding surfaces of the CENP-T-Mis12C are identified
- The Dsn1 basic motif inhibits the CENP-T-Mis12C interaction during interphase
- Dual phosphoregulation of Dsn1 and CENP-T ensures robust kinetochore assembly

Authors

Yusuke Takenoshita, Masatoshi Hara, Reiko Nakagawa, Mariko Ariyoshi, Tatsuo Fukagawa

Correspondence

fukagawa.tatsuo.fbs@osaka-u.ac.jp

In brief

Biological sciences; Cell biology; Biophysics

Takenoshita et al., 2024, iScience *27*, 111295
December 20, 2024
https://doi.org/10.1016/j.isci.2024.111295

CellPress

iScience

CellPress
OPEN ACCESS

Article

Molecular details and phosphoregulation of the CENP-T-Mis12 complex interaction during mitosis in DT40 cells

Yusuke Takenoshita,[1] Masatoshi Hara,[1] Reiko Nakagawa,[2] Mariko Ariyoshi,[1] and Tatsuo Fukagawa[1,3,*]
[1]Graduate School of Frontier Biosciences, Osaka University, Suita, Osaka 565-0871, Japan
[2]RIKEN Center for Biosystems Dynamics Research, Kobe, Hyogo 650-0047, Japan
[3]Lead contact
*Correspondence: fukagawa.tatsuo.fbs@osaka-u.ac.jp
https://doi.org/10.1016/j.isci.2024.111295

SUMMARY

To establish bipolar attachments of microtubules to sister chromatids, an inner kinetochore subcomplex, the constitutive centromere-associated network (CCAN), is assembled on centromeric chromatin and recruits the microtubule-binding subcomplex called the KMN network. Since CCAN proteins CENP-C and CENP-T independently bind to the Mis12 complex (Mis12C) of KMN, it is difficult to evaluate the significance of each interaction in cells. Here, we demonstrate the molecular details of the CENP-T-Mis12C interaction using chicken DT40 cells lacking the CENP-C-Mis12C interaction. Using AlphaFold predictions combined with cell biological and biochemical analyses, we identified three binding surfaces of the CENP-T-Mis12C interaction, demonstrating that each interface is important for recruiting Mis12C to CENP-T in cells. This interaction, via three interaction surfaces, is cooperatively regulated by dual phosphorylation of Dsn1 (a Mis12C component) and CENP-T, ensuring a robust CENP-T-Mis12C interaction and proper mitotic progression. These findings deepen our understanding of kinetochore assembly in cells.

INTRODUCTION

Chromosome segregation during mitosis is critical for transmitting genetic information to the progeny. This is achieved by attaching sister chromatids to bipolar mitotic spindles, leading to chromosome segregation into daughter cells. Spindle microtubules bind to a large protein complex called the kinetochore, which is formed on the centromere of each sister chromatid to ensure accurate chromosome segregation.[1–4] To understand the mechanisms underlying chromosome segregation, it is crucial to clarify how the kinetochore is assembled on the centromere.

Kinetochores comprise two major complexes. One is the constitutive centromere-associated network (CCAN), containing 16 protein components that constitutively localize to the centromere throughout the cell cycle, forming a base for kinetochore assembly.[2,3,5–10] Another large complex is the KMN network, comprising the Knl1 complex (Knl1C), Mis12 complex (Mis12C), and Ndc80 complex (Ndc80C), which are associated with CCAN from G_2 phase to mitosis to establish a functional kinetochore structure for spindle microtubule binding.[2,6–8] Ndc80C in the KMN network directly associates with spindle microtubules,[11–13] and also associates with CCAN directly or via Mis12C.[2,7,8] Since CCAN associates with centromeric chromatin, the linkage between CCAN and the KMN network is critical for bridging centromeric chromatin with spindle microtubules, ultimately ensuring accurate chromosome segregation.

In vertebrate cells, the KMN network is recruited to the CCAN through two parallel pathways: the CENP-C and CENP-T pathways.[1,3,4,6,14–20] Mis12C binds to CENP-C and CENP-T independently in each pathway, acting as a hub for KMN network assembly by recruiting Ndc80C and Knl1C.[21] In addition, CENP-T directly recruits Ndc80C via the Ndc80C binding domain(s) at its N-terminus (human CENP-T has two binding domains and chicken CENP-T has one domain).[15,17,22] Although both pathways contribute to Mis12C recruitment for KMN network assembly at an appropriate time,[16–18,23,24] the CENP-T-Mis12C interaction has a dominant function in chromosome segregation compared to the CENP-C-Mis12C interaction in chicken DT40 cells.[18,24] Previous studies have proposed a molecular basis for the human CENP-T-Mis12C interaction based on *in vitro* binding assays and structural prediction analyses.[22,25,26] However, it remains unclear how the CENP-T-Mis12C interaction is regulated and how this regulatory mechanism is significant in cells, as it is challenging to distinguish CENP-C- and CENP-T-binding Mis12C in native kinetochores. Therefore, clarifying the regulatory mechanisms and biological significance of CENP-T-Mis12C interaction in cells is not trivial.

In this study, we examined the molecular details of the CENP-T-Mis12C interaction at the native kinetochore using chicken DT40 mutant cells lacking the Mis12C binding region of CENP-C. Combined with structure prediction and cell biology analyses, we identified two binding sites in CENP-T for Mis12C interaction, which are essential for DT40 cell viability. In addition,

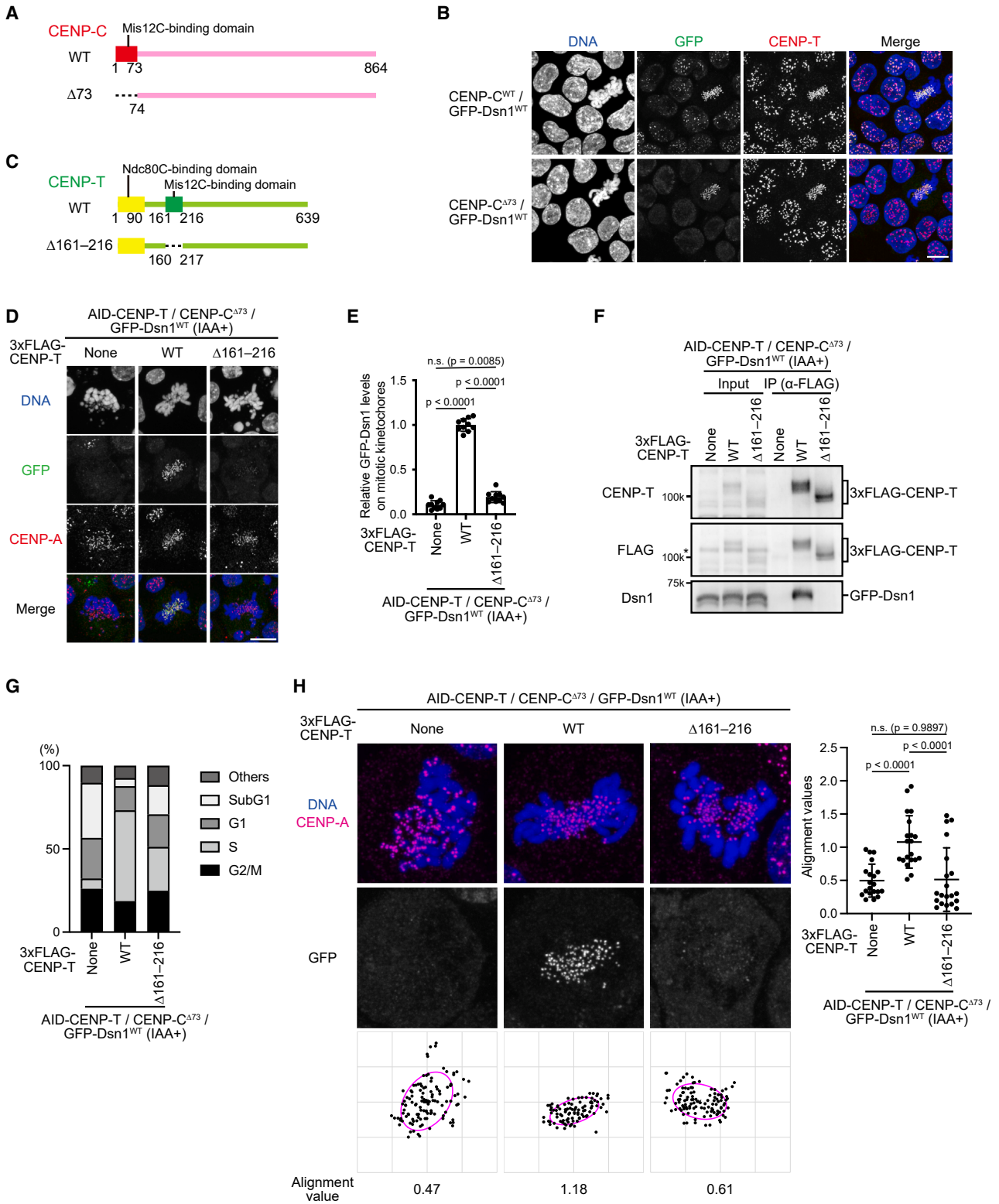

(legend on next page)

a third region of CENP-T seems to contribute to the binding to Mis12C when CENP-T is phosphorylated. We also propose that the dual phosphorylation of Dsn1 and CENP-T cooperatively facilitates the CENP-T-Mis12C interaction, ensuring mitotic progression in DT40 cells. The molecular details of the dual phosphoregulation of the CENP-T-Mis12C interaction provide insights into the robust assembly mechanism of kinetochores for accurate chromosome segregation.

RESULTS

Localization profile of CENP-C- and CENP-T-binding Mis12C in chicken DT40 cells

Both CENP-C and CENP-T contain a binding region for Mis12C[14,15,18,22,24,25,27,28]; however, it is unclear when and how Mis12C is recruited to each binding region. To distinguish the cell cycle timing of Mis12C recruitment to CENP-C and CENP-T, we examined Mis12C localization at kinetochores in CENP-C^{WT} cells (wild-type chicken DT40 cells) and CENP-$C^{\Delta 73}$ cells lacking the Mis12C-binding region of CENP-C (aa 1–73; Figures 1A and S1A). Although depletion of CENP-C leads to chromosome segregation defect due to loss of interactions with various kinetochore proteins,[29,30] the Mis12C-binding region of CENP-C is dispensable for chromosome segregation in chicken DT40 cells.[18] Therefore, CENP-$C^{\Delta 73}$ cells enable the observation of CENP-T-bound Mis12C at the native kinetochore. To visualize Mis12C, we introduced a GFP-Dsn1 construct (a Mis12C component) into the endogenous Dsn1 locus (Figures S1B–S1E). Consistent with our previous findings showing that Mis12C starts to localize to centromeres in interphase and continues to localize during mitosis in chicken DT40 cells,[18] GFP-Dsn1 localized to centromeres in both interphase and M phase in CENP-C^{WT} cells (Figure 1B). However, GFP-Dsn1 localized to centromeres only during mitosis and not during interphase in CENP-$C^{\Delta 73}$ cells (Figure 1B), suggesting that Mis12C associates only with CENP-C and does not bind to CENP-T in interphase cells.

Previous studies have suggested that the Dsn1 basic motif stabilizes a Mis12C auto-inhibited state,[26,31] which prevents the CENP-C-Mis12C interaction during interphase. The Mis12C auto-inhibited state is relieved by phosphorylation of the Dsn1 basic motif by the mitotic kinase Aurora B during mitosis.[18,26,28,31] However, Mis12C was recruited to CENP-C in the interphase of DT40 cells (Figure 1B), suggesting that CENP-C binds to Mis12C in the auto-inhibited state. To examine the molecular basis of the chicken CENP-C-Mis12C interaction, we utilized AlphaFold2 to predict the structure of Mis12C, including four full-length proteins (Mis12, Nsl1, Dsn1, and Pmf1) in complex with CENP-C aa 1–73 (the Mis12C-binding region). The predicted structure of chicken Mis12C comprised two head domains (Head1: composed of Mis12 and Pmf1; and Head2: composed of Dsn1 and Nsl1) connected to a coiled-coil stalk domain, which is composed of Mis12, Pmf1, Dsn1, and Nsl1. This structure is similar to the crystal structures of human and yeast Mis12C.[28,32] The structure suggests that the Dsn1 basic motif binds to both Head1 and Head2 of Mis12C to form the auto-inhibited Mis12C state, consistent with the cryo-EM structure of the human KMN complex (Figures S1G and S1H).[26] The Predicted Aligned Error (PAE) suggests that the aa 1–21 and aa 22–42 regions of CENP-C bind to Mis12C in the auto-inhibited state (Figures S1I and S1J). The aa 1–21 region of CENP-C may bind to Mis12C through Nsl1 and Mis12 (pLDDT <50; Figures S1J and S1K). However, the comparison between the crystal structure of human Mis12C in complex with CENP-C[28] and the cryo-EM structure of the human KMN complex[26,31] suggests that the N-terminus of human CENP-C, which corresponds to the aa 1–21 of chicken CENP-C, causes a steric clash with the basic motif of human Dsn1. Similar to the human case, it is possible that the aa 1–21 of chicken CENP-C might also cause a steric clash with the basic motif of Dsn1. The aa 22–42 region of CENP-C also binds to Mis12C through Pmf1 and Mis12 (90 > pLDDT >50; Figures S1J and S1K). Even if the aa 1–21 region of CENP-C causes a steric clash with the Dsn1 basic motif, the Mis12C-CENP-C interaction should be maintained using the aa 22–42 region of CENP-C. This finding is consistent with previous *in vitro* binding assay showing that human CENP-C binds to human Mis12C in the auto-inhibited state.[26]

We previously demonstrated that Tet-off-based CENP-T conditional knockout CENP-$C^{\Delta 73}$ cells expressing CENP-$T^{\Delta 161–200}$ or CENP-$T^{\Delta 201–216}$ showed a significant reduction in Mis12C

Figure 1. CENP-T interacts with Mis12C during mitosis in chicken DT40 cells

(A) Schematic representation of chicken CENP-C (864 aa). The Mis12C-binding domain was deleted in CENP-$C^{\Delta 73}$.

(B) Localization of GFP-Dsn1 in CENP-C^{WT} and CENP-$C^{\Delta 73}$ cells. Cells were fixed and stained with an anti-CENP-T antibody. DNA was stained with DAPI. Scale bar, 10 μm.

(C) Schematic representation of chicken CENP-T (639 aa). The Mis12C-binding domain was deleted in CENP-$T^{\Delta 161–216}$.

(D) Localization of GFP-Dsn1. 3xFLAG-CENP-T^{WT} or 3xFLAG-CENP-$T^{\Delta 161–216}$ was expressed in AID-based CENP-T conditional knockdown CENP-$C^{\Delta 73}$ cells in which wild-type CENP-T protein was degraded by IAA addition. Cells were treated with IAA for 12 h, fixed, and stained with an anti-CENP-A antibody. DNA was stained with DAPI. Scale bar, 10 μm.

(E) Quantification data of GFP-Dsn1 signals at kinetochores in mitotic cells shown in (D). Error bars show the mean ± SD; *p*-values were calculated by one-way ANOVA ($F(2,27) = 672.4$; $p < 0.0001$) followed by Tukey's test.

(F) Immunoprecipitation using anti-FLAG antibody in AID-based CENP-T conditional knockdown CENP-$C^{\Delta 73}$/GFP-Dsn1 cells expressing 3xFLAG-CENP-T^{WT} or 3xFLAG-CENP-$T^{\Delta 161–216}$. Cells were cultured with IAA for 12 h and nocodazole was added for last 10 h before immunoprecipitation experiments. Immunoprecipitated samples were subjected to immunoblot analyses using anti-CENP-T, anti-FLAG, and anti-Dsn1 antibodies. Asterisk indicates nonspecific bands.

(G) Cell cycle distribution profiles of AID-based CENP-T conditional knockdown CENP-$C^{\Delta 73}$/GFP-Dsn1 cells expressing 3xFLAG-CENP-T^{WT} or 3xFLAG-CENP-$T^{\Delta 161–216}$ in the presence of IAA for 12 h.

(H) Chromosome alignment values in AID-based CENP-T conditional knockdown CENP-$C^{\Delta 73}$/GFP-Dsn1 cells expressing 3xFLAG-CENP-T^{WT} or 3xFLAG-CENP-$T^{\Delta 161–216}$ in the presence of IAA for 12 h and MG132 for the last 2 h. Error bars show the mean ± SD; *p*-values were calculated by one-way ANOVA ($F(2,57) = 14.78$; $p < 0.0001$) followed by Tukey's test.

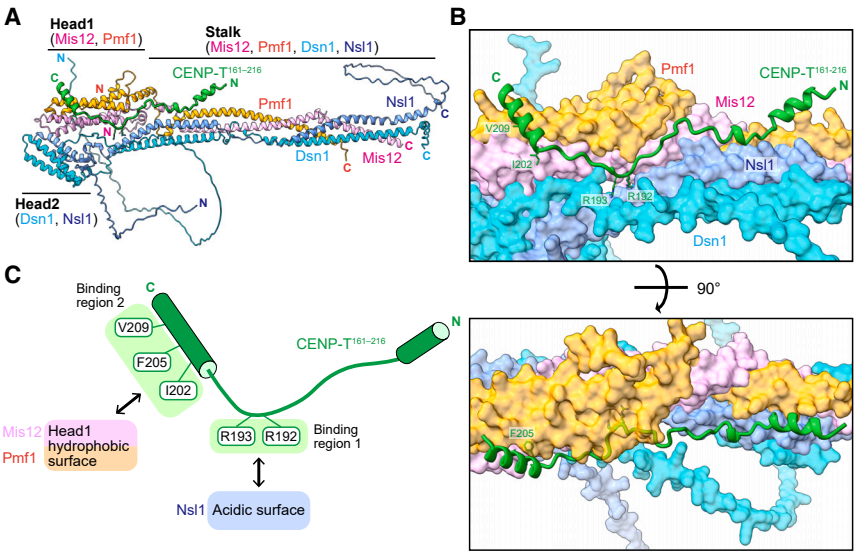

Figure 2. Molecular basis for the chicken CENP-T-Mis12C interaction based on a complex structure predicted by AlphaFold2

(A) AlphaFold2 predicted structure of chicken Mis12C in complex with the Mis12C-binding domain of CENP-T (rank_1 model; rank_2, 3, 4, and 5 models are shown in Figure S3). The CENP-T aa 161–216 region and the full lengths of Mis12C components (Mis12, Nsl1, Dsn1, and Pmf1) were used for the prediction, displayed as a cartoon, and color-coded as indicated in the figure.

(B) Overview of the CENP-T-Mis12C interface. Mis12C is shown as a surface model, and the CENP-T aa 161–216 region is shown as a cartoon. The side chains of key residues of CENP-T for binding to Mis12C are shown with labels.

(C) Schematic representation of the CENP-T aa 161–216 structure. There are two binding regions for Mis12C (binding regions 1 and 2). Binding region 1 interacts with the acidic surface of Nsl1, and binding region 2 binds to the Head1 region of Mis12C via hydrophobic interactions.

localization at kinetochores compared to CENP-C$^{\Delta 73}$ cells expressing CENP-T^{WT}.[24] This suggests that both the aa 161–200 and aa 201–216 regions of CENP-T are important for interaction with Mis12C. To efficiently examine the molecular mechanisms of interaction between CENP-T and Mis12C at centromeres using CENP-C$^{\Delta 73}$ cells, we used Auxin-Inducible Degron (AID)-based knockdown cells, instead of Tet-off-based knockout cells. We expressed AID-tagged CENP-T and introduced an FLAG-fused CENP-T mutant construct lacking the aa 161–216 region into the endogenous CENP-T locus in CENP-C$^{\Delta 73}$ cells (CENP-C$^{\Delta 73}$/CENP-T$^{\Delta 161–216}$ cells; Figures 1C and S2A–S2H). In this cell line, wild-type CENP-T was degraded after 3-indole acetic acid (IAA) addition, and instead of wild-type CENP-T, only CENP-T$^{\Delta 161–216}$ was expressed (Figure S2H). As a control, the FLAG-fused wild-type CENP-T construct was introduced into the CENP-T locus (CENP-C$^{\Delta 73}$/CENP-T^{WT} cells; Figures S2F–S2H). Next, we examined the mitotic localization of Mis12C in these cells. The mitotic GFP-Dsn1 localization observed in CENP-C$^{\Delta 73}$/CENP-T^{WT} cells was almost undetectable in CENP-C$^{\Delta 73}$/CENP-T$^{\Delta 161–216}$ cells (Figures 1D and 1E). Although AID-fused CENP-T is not completely degraded after IAA addition (Figure S2H), the Mis12C levels at the kinetochore reduced to ~15% in CENP-C$^{\Delta 73}$/CENP-T$^{\Delta 161–216}$ cells (Figure 1E), suggesting the AID-based CENP-T knockdown cells are appropriate for the following experiments. Consistent with this result, Mis12C co-immunoprecipitated with CENP-T^{WT} but not with CENP-T$^{\Delta 161–216}$ (Figure 1F). In addition to the CENP-T-Mis12C interaction data, we examined the cell cycle profile of CENP-C$^{\Delta 73}$/CENP-T$^{\Delta 161–216}$ cells by flow cytometry. The G2/M, SubG1, and Others fractions were increased in CENP-C$^{\Delta 73}$/CENP-T$^{\Delta 161–216}$ cells, similar to AID-based CENP-T knockdown in CENP-C$^{\Delta 73}$ cells (Figures 1G and S2I), suggesting that mitotic (G2/M) arrest and subsequent cell death (SubG1 and Others) occurred in CENP-C$^{\Delta 73}$/CENP-T$^{\Delta 161–216}$ cells. To further analyze the mitotic phenotype of CENP-C$^{\Delta 73}$/CENP-T$^{\Delta 161–216}$ cells, we examined the chromosome alignment of mitotic cells. As shown in Figure 1H, chromosomes were well aligned in the metaphase plate in CENP-C$^{\Delta 73}$/CENP-T^{WT} cells, whereas chromosomes were not aligned in CENP-C$^{\Delta 73}$/CENP-T$^{\Delta 161–216}$ cells and AID-based CENP-T knockdown CENP-C$^{\Delta 73}$ cells. Taken together, we propose that the aa 161–216 region of CENP-T is required for Mis12C mitotic kinetochore localization via CENP-T-Mis12C interaction in CENP-C$^{\Delta 73}$ cells and is critical for proper mitotic progression due to its binding to Mis12C.

Structural prediction of interfaces for the chicken CENP-T-Mis12C interaction

Next, to examine the molecular basis of the chicken CENP-T-Mis12C interaction, we utilized AlphaFold2 to predict the structure of Mis12C, including four full-length proteins (Mis12, Nsl1, Dsn1, and Pmf1) in complex with the aa 161–216 region of CENP-T (Figures 2A and S3A–S3D). The predicted structure of Mis12C were similar to the structure of Mis12C complexed with CENP-C. The model of CENP-T$^{161–216}$ contains two α-helices connected via an extended linker region.

AlphaFold2 predicted that CENP-T$^{161–216}$ binds across the stalk domain to the Head1 domain of Mis12C (Figures 2A, 2B, and S3C–S3E). The pLDDT scores indicate that the aa 161–186 region of CENP-T has lower confidence (pLDDT <70), whereas the aa 187–216 region has higher confidence (pLDDT >70) and adopts a more reliable structure (Figure S3E). The PAE also shows that the aa 187–216 region of CENP-T binds to Mis12C with high reliability (Figure S3C; rank_1). The predicted structure suggested two main Mis12C-binding regions of CENP-T (binding region 1 and 2; Figures 2B and 2C). In the binding region 1, R192 and R193 of CENP-T (90 > pLDDT >70) in the extended region is supposed to interact with the Nsl1 acidic surface in the stalk region of Mis12C (Figures 2B and 2C). In the binding region 2, the C-terminal α-helix of CENP-T$^{161–216}$ harboring I202, F206, and V209 (100 > pLDDT >70) is predicted to associate with the hydrophobic surface of the Head1 domain of Mis12C

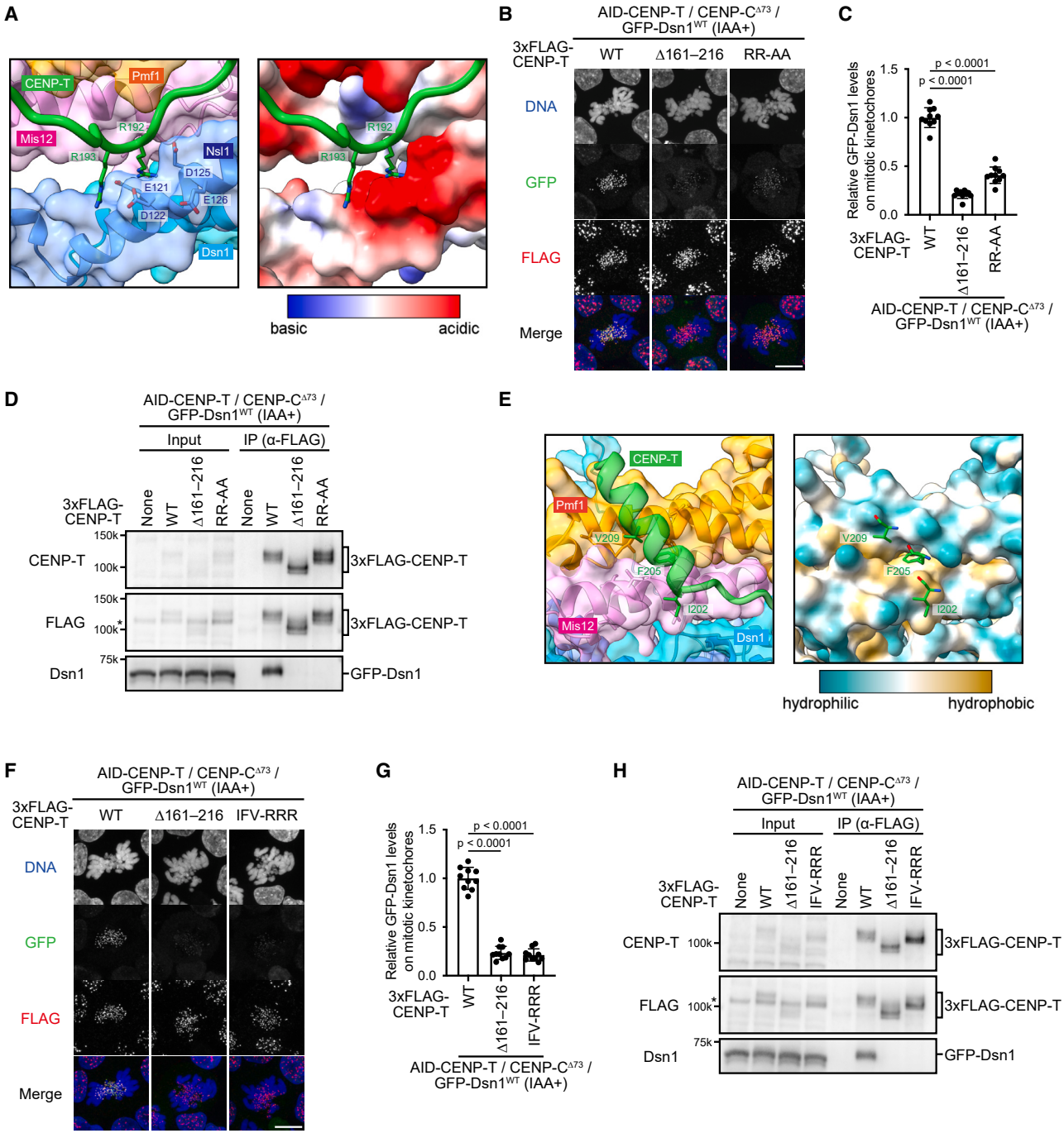

Figure 3. Two binding regions of CENP-T are required for the chicken CENP-T-Mis12C interaction

(A) The magnified view of the Nsl1 acidic surface associated with the binding region 1 of CENP-T. Left: The transparent surface model of Mis12C is overlaid on a cartoon model. CENP-T is shown as a cartoon and models are color-coded as indicated in the figure. CENP-T R192 and R193 and Nsl1 acidic residues (E121, D122, D125, and E126) are labeled. Right: Electrostatic potential of Mis12C mapped on the surface representation. CENP-T is shown as a cartoon.

(B) Localization of GFP-Dsn1. 3xFLAG-CENP-T^{WT}, 3xFLAG-CENP-T$^{\Delta 161–216}$, or 3xFLAG-CENP-T^{RR-AA} was expressed in AID-based CENP-T conditional knockdown CENP-C$^{\Delta 73}$ cells in which wild-type CENP-T protein was degraded by IAA addition. Cells were treated with IAA for 12 h, fixed, and stained with an anti-FLAG antibody. DNA was stained with DAPI. Scale bar, 10 μm.

(C) Quantification data of GFP-Dsn1 signals at kinetochores in mitotic cells shown in (B). Error bars show the mean ± SD; *p*-values were calculated by one-way ANOVA ($F(2,27) = 262.6$; $p < 0.0001$) followed by Tukey's test.

(D) Immunoprecipitation using anti-FLAG antibody in AID-based CENP-T conditional knockdown CENP-C$^{\Delta 73}$/GFP-Dsn1 cells expressing 3xFLAG-CENP-T^{WT}, 3xFLAG-CENP-T$^{\Delta 161–216}$, or 3xFLAG-CENP-T^{RR-AA}. Cells were cultured with IAA for 12 h and nocodazole was added for last 10 h before immunoprecipitation

(legend continued on next page)

(Figures 2B and 2C). The AlphaFold2 predicted structure of human Mis12C in complex with the aa 176–232 region of human CENP-T is similar to the predicted structure of chicken Mis12C in complex with chicken CENP-T$^{161–216}$ (Figures S3F–S3I). As these two Mis12C-binding regions of CENP-T seem important for the CENP-T-Mis12C interaction, we further analyzed the molecular details of the CENP-T-Mis12C interaction and its significance in CENP-C$^{\Delta73}$ DT40 cells.

Electrostatic interaction of Mis12C with the binding region 1 of CENP-T

As described above, the AlphaFold2 model suggested that the two arginine residues of CENP-T (R192 and R193) in the binding region 1 form electrostatic interactions with the acidic surface of Nsl1 in Mis12C (Figure 3A). These arginine residues of CENP-T and the acidic region of Nsl1 are highly conserved (Figures S4A and S4B). Human CENP-T residues R209 and R210, corresponding to R192 and R193 of chicken CENP-T, are predicted to bind to the acidic surface of human Nsl1 (Figure S3H). To evaluate the importance of this interaction surface in chicken DT40 cells, we replaced R192 and R193 with alanine in CENP-T (CENP-T^{RR-AA}) and introduced a mutant construct into the CENP-T locus in CENP-C$^{\Delta73}$ cells expressing AID-CENP-T (CENP-C$^{\Delta73}$/CENP-T^{RR-AA} cells; Figure S4C). We examined the GFP-Dsn1 levels at the mitotic kinetochores in these cells and found that these levels were ~35% of those in CENP-C$^{\Delta73}$/CENP-T^{WT} cells, which were slightly higher than that in CENP-C$^{\Delta73}$/CENP-T$^{\Delta161–216}$ cells (Figures 3B and 3C). We also confirmed that Mis12C did not co-precipitate with CENP-T^{RR-AA} like CENP-T$^{\Delta161–216}$ (Figure 3D). Consistent with these results, we observed a clear growth delay in CENP-C$^{\Delta73}$/CENP-T^{RR-AA} cells following IAA addition (Figure S4D). Although we cannot completely rule out the possibility that CENP-T^{RR-AA} indirectly reduced Mis12C binding, we propose that CENP-T R192 and R193 form electrostatic interactions with the Nsl1 acidic region, which is important for the CENP-T-Mis12C binding and cell proliferation.

Hydrophobic interaction of Mis12C with the binding region 2 of CENP-T

Structure prediction also suggested that the hydrophobic residues of CENP-T (I202, F205, and V209) aligning on the α-helix in the binding region 2 were associated with the hydrophobic surface of the Mis12C Head1 domain (Figure 3E). Although the hydrophobic residues of CENP-T are not thoroughly conserved in other species, the corresponding regions in human and mouse CENP-T contain a cluster of hydrophobic residues (Figure S4A). The human CENP-T residues V219, F222, and L226, corresponding to I202, F205, and V209 of chicken CENP-T, are predicted to bind to the hydrophobic region of human Mis12C Head1 domain (Figure S3I). To evaluate the importance of this hydrophobic interface, we replaced I202, F205, and V209 of chicken CENP-T with arginine (CENP-T$^{IFV-RRR}$) and introduced a mutant construct into the CENP-T locus of CENP-C$^{\Delta73}$ cells expressing AID-fused CENP-T (CENP-C$^{\Delta73}$/CENP-T$^{IFV-RRR}$ cells; Figure S4E). We observed a significant reduction in GFP-Dsn1 levels in the mitotic kinetochores of CENP-C$^{\Delta73}$/CENP-T$^{IFV-RRR}$ cells compared to those of CENP-C$^{\Delta73}$/CENP-T^{WT} cells (Figures 3F and 3G), and Mis12C did not co-precipitate with CENP-T$^{IFV-RRR}$ (Figure 3H). As in the case of CENP-C$^{\Delta73}$/CENP-T$^{\Delta161–216}$ cells, after IAA addition, CENP-C$^{\Delta73}$/CENP-T$^{IFV-RRR}$ cells stopped growing and ultimately died (Figure S4D). As the case of CENP-T^{RR-AA} mutant, we cannot rule out the possibility that CENP-T$^{IFV-RRR}$ may indirectly cause reduction of Mis12C-binding. However, our results strongly suggest that the hydrophobic interaction of the binding region 2 of CENP-T with Mis12C is critical for the CENP-T-Mis12C binding and cell viability.

In summary, CENP-T has at least two binding regions for Mis12C, each important for its binding to Mis12C. This result is consistent with our previous finding that either the CENP-T aa 161–200 (containing binding region 1) or the aa 201–216 (containing binding region 2) is required for CENP-T function via binding to Mis12C.[24]

Phosphorylation of Dsn1 in Mis12C facilitates stable CENP-T-Mis12C interaction

Although CENP-C interacts with Mis12C in both interphase and M phase, CENP-T interacts with Mis12C during mitosis but not in interphase (Figure 1). This implies that there are regulatory mechanisms by which CENP-T binds to Mis12C only during mitosis. The structural model of the human KMN complex suggests that the Dsn1 basic motif binds to the Head1 and Head2 of Mis12C, which forms the closed conformation of the Head domains and masks the Nsl1 acidic surface (auto-inhibited state).[26,31] The corresponding region of chicken Nsl1 is recognized by the CENP-T binding region 1 (Figure 3A). Our AlphaFold2 prediction model for chicken Mis12C also suggests that the Dsn1 basic motif binds to the Head2 of Mis12C via K110 in the RKSL motif (R109, K110, S111, and L112)[26] and the

experiments. Immunoprecipitated samples were subjected to immunoblot analyses using anti-CENP-T, anti-FLAG, and anti-Dsn1 antibodies. Asterisk indicates nonspecific bands.

(E) Magnified view of the Mis12C-Head1 hydrophobic surface interacting with the binding region 2 of CENP-T. Left: The transparent surface model of Mis12C is overlaid on a cartoon model. CENP-T is shown as a cartoon and models are color-coded as indicated in the figure. CENP-T I202, F205, and V209 are labeled. Right: Hydrophobic potential of Mis12C mapped on the surface representation. CENP-T I202, F205, and V209 are shown as sticks.

(F) Localization of GFP-Dsn1. 3xFLAG-CENP-T^{WT}, 3xFLAG-CENP-T$^{\Delta161–216}$, or 3xFLAG-CENP-T$^{IFV-RRR}$ was expressed in AID-based CENP-T conditional knockdown CENP-C$^{\Delta73}$ cells. Cells were treated with IAA for 12 h, fixed, and stained with an anti-FLAG antibody. DNA was stained with DAPI. Scale bar, 10 μm.

(G) Quantification data of GFP-Dsn1 signals at kinetochores in mitotic cells shown in (F). Error bars show the mean ± SD; p-values were calculated by one-way ANOVA ($F(2,27) = 284.8$; $p < 0.0001$) followed by Tukey's test.

(H) Immunoprecipitation using anti-FLAG antibody in AID-based CENP-T conditional knockdown CENP-C$^{\Delta73}$/GFP-Dsn1 cells expressing 3xFLAG-CENP-T^{WT}, 3xFLAG-CENP-T$^{\Delta161–216}$, or 3xFLAG-CENP-T$^{IFV-RRR}$. Cells were cultured with IAA for 12 h and nocodazole was added for last 10 h before immunoprecipitation experiments. Immunoprecipitated samples were subjected to immunoblot analyses using anti-CENP-T, anti-FLAG, and anti-Dsn1 antibodies. Asterisk indicates nonspecific bands.

hydrophobic pocket of Head1 (Mis12 and Pmf1) and acidic surface of Nsl1 via the WRR linchpin (W98, R99, and R100)[26] and additional lysine residue (K104; Figure 4A). These interactions might result in Mis12C adopting an auto-inhibited state. The Dsn1 basic motif possesses Aurora B phosphorylation sites,[16,33] and phosphorylation by Aurora B at these sites inhibits the binding of the Dsn1 basic motif to the Head domains of Mis12C.[26,28,31,32] Thus, the interaction between the binding region 1 of CENP-T and the Nsl1 acidic surface might be inhibited by the Dsn1 basic motif during interphase; this inhibition is released during mitosis by Aurora B phosphorylation, similarly to the CENP-C-Mis12C interaction.[18,28,32] Although this possibility was discussed based on an *in vitro* binding assay and structural model of human Mis12C,[25,26] it is unclear whether this mechanism regulates the CENP-T-Mis12C interaction in cells. To test this hypothesis, we generated a Dsn1 construct lacking the basic motif (aa 93–114; Dsn1$^{\Delta 93-114}$) and introduced it into the endogenous Dsn1 locus of CENP-C$^{\Delta 73}$ cells (Figures 4B, S1D, and S5A). While Dsn1^{WT} localized to kinetochores only during mitosis, Dsn1$^{\Delta 93-114}$ localized to both interphase and mitotic kinetochores in CENP-C$^{\Delta 73}$ cells (Figure 4C), suggesting that the Dsn1 basic motif inhibits the CENP-T-Mis12C interaction during interphase. While other mechanisms that inhibit the CENP-T-Mis12C interaction during interphase cannot be ruled out, the inhibitory effect of the Dsn1 basic motif is significant. Since both binding region 1 and 2 of CENP-T are important for the Mis12C binding (Figure 3), CENP-T seems to interact with Mis12C via binding region 1 and 2 in CENP-C$^{\Delta 73}$/Dsn1$^{\Delta 93-114}$ interphase cells. Combined, we propose that the Dsn1 basic motif masks the binding surface of Mis12C for binding region 1 of CENP-T, and the mask is released upon phosphorylation, leading to the interaction between binding region 1 of CENP-T and Mis12C during mitosis. In turn, the release of the mask also facilitates the interaction between binding region 2 of CENP-T and Mis12C (Figure S5B). These results suggest a linkage between the regulatory mechanisms governing the interactions of binding region 1 and 2 of CENP-T with Mis12C.

Next, we generated Dsn1^{4A}, in which the four Aurora B phosphorylation sites of Dsn1 (Figure S5A) were substituted with alanine and introduced into the endogenous Dsn1 locus in CENP-C$^{\Delta 73}$ cells expressing AID-fused CENP-T (CENP-C$^{\Delta 73}$/Dsn1^{4A} cells; Figures S2D, S2G, and S5C). We quantified the GFP-Dsn1 levels in these cells and found that they were reduced to approximately 55% relative to CENP-C$^{\Delta 73}$/Dsn1^{WT} cells (Figures 4D and 4E). We also demonstrated that Dsn1^{4A} did not co-precipitate well with CENP-T compared with Dsn1^{WT} (Figure 4F). The growth of CENP-C$^{\Delta 73}$/Dsn1^{4A} cells was comparable to that of CENP-C$^{\Delta 73}$/Dsn1^{WT} cells (Figure S5D), suggesting that half of the Dsn1 was sufficient for the viability of CENP-C$^{\Delta 73}$ cells. The expression of Dsn1^{4A} did not drastically suppress Mis12C localization during mitosis in CENP-C$^{\Delta 73}$ cells unlike the expression of CENP-T^{RR-AA} (with mutations in binding region 1 of CENP-T). Since the presence of the Dsn1 basic motif completely suppresses the Mis12C localization to kinetochores during interphase in CENP-C$^{\Delta 73}$ cells (Figure 4C), in addition to phosphorylation of the Dsn1 basic motif by Aurora B, there should be a regulatory mechanism for the CENP-T-Mis12C interaction.

CENP-T phosphorylation is involved in the regulation of the CENP-T-Mis12C interaction

As the additional regulatory mechanism for the CENP-T-Mis12C interaction, CENP-T-mediated phosphorylation is one of the candidates because chicken CENP-T is highly phosphorylated during mitosis.[24] First, we examined the phosphorylation sites in the CENP-T aa 161–216 region using mitotic DT40 cell extracts by mass spectrometry and found that S175 and T184 were phosphorylated during mitosis (Figures 5A and S6A). T184 in chicken CENP-T might correspond to S201 of human CENP-T, which is phosphorylated by CDK1[22,25]; however, surrounding sequences of S175 in chicken CENP-T are not clearly conserved in other species (Figure S4A), and it is unclear which mitotic kinase phosphorylates this site. As these two residues were not included in the binding regions 1 and 2, we re-evaluated the AlphaFold 2 prediction model of Mis12C in complex with the aa 161–216 region of CENP-T. As shown in Figure 5B, S175 and T184 are close to the basic regions of Nsl1 and Pmf1, suggesting that phosphorylation of these CENP-T residues might provide the additional Mis12C binding sites mediated via electrostatic interactions and stabilize the CENP-T-Mis12C interface. On the other hand, the AlphaFold3 prediction with phosphorylated S175 and T184 suggested that Mis12C might not directly interact with phosphorylated S175 and T184 of CENP-T (Figures S6B and S6C), but the spatial proximity of the charges might still have a significant effect on the affinity. We generated a CENP-T mutant construct in which S175 and T184 were substituted with alanine and introduced into the CENP-T locus in CENP-C$^{\Delta 73}$ cells expressing AID-fused CENP-T (CENP-C$^{\Delta 73}$/CENP-T^{2A} cells; Figures S2G and S6D). We examined GFP-Dsn1 levels at kinetochores in CENP-C$^{\Delta 73}$/CENP-T^{2A} cells and found that GFP-Dsn1 levels were significantly reduced compared to those in CENP-C$^{\Delta 73}$/CENP-T^{WT} cells ($\sim$70% of those in CENP-C$^{\Delta 73}$/CENP-T^{WT} cells; Figures 5C and 5D). We also found that the levels of Mis12C that co-precipitated with CENP-T^{2A} were lower than those with CENP-T^{WT} (Figure 5E). These results are consistent with previous studies that showed phosphorylation of human CENP-T facilitates its interaction with Mis12C *in vitro*.[22,25] Based on these results, we propose that CENP-T phosphorylation contributed to facilitating the CENP-T-Mis12 interaction (Figure S6E; see discussion). However, as in the case of CENP-C$^{\Delta 73}$/Dsn1^{4A} cells, substantial growth defects were not observed in CENP-C$^{\Delta 73}$/CENP-T^{2A} cells (Figure S6F), indicating that CENP-C$^{\Delta 73}$ cells are still viable even when the interaction between CENP-T phospho-sites and Mis12C is impaired.

Double mutant cells expressing CENP-T^{2A} and Dsn1^{4A} cause a more substantial reduction of Mis12C levels at kinetochores than single mutant cells

Although phosphorylation of Dsn1 and CENP-T facilitates the CENP-T-Mis12C interaction at different binding interfaces, inhibition of either phosphorylation did not impair CENP-C$^{\Delta 73}$ cell proliferation. This prompted us to examine the phenotype of double mutant cells expressing CENP-T^{2A} and Dsn1^{4A}. We introduced a construct containing either GFP-Dsn1^{WT} or GFP-Dsn1^{4A} into the endogenous Dsn1 locus of CENP-C$^{\Delta 73}$/CENP-T^{2A} cells (Figures S2G and S7A). We then analyzed the effect

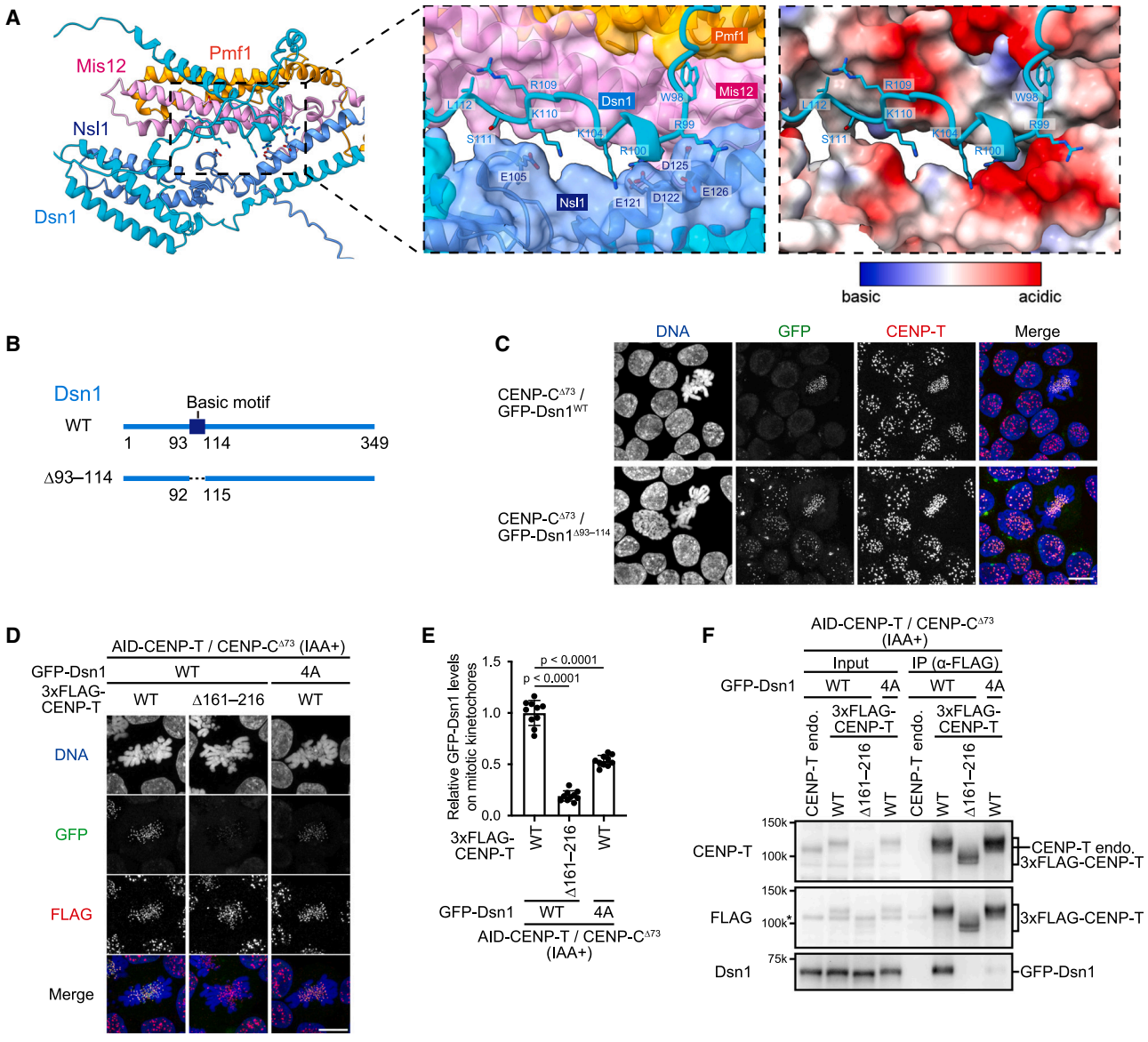

Figure 4. The Dsn1 basic motif regulates the chicken CENP-T-Mis12C interaction

(A) Overview of the Mis12C auto-inhibited state in the AlphaFold2 predicted structure of chicken Mis12C. Left: Mis12C is shown as a cartoon and color-coded, as indicated in the figure. Middle: The transparent surface model of Mis12C, except for the basic motif of Dsn1, is overlaid on a cartoon model. The basic motif of Dsn1 is shown as a cartoon. The key residues of Dsn1 important for maintaining the auto-inhibited state are labeled. Right: Electrostatic potential of Mis12C, except for the basic motif of Dsn1, mapped on the surface representation. The basic motif of Dsn1 is shown as a cartoon.

(B) Schematic representation of chicken Dsn1 (349 aa). The basic motif was deleted in Dsn1$^{\Delta 93-114}$. Amino acid sequences are shown in Figure S5A.

(C) Localization of GFP-Dsn1^{WT} or GFP-Dsn1$^{\Delta 93-114}$ in CENP-C$^{\Delta 73}$ cells. Cells were fixed and stained with an anti-CENP-T antibody. DNA was stained with DAPI. Scale bar, 10 μm.

(D) Localization of GFP-Dsn1. GFP-Dsn1^{WT} or GFP-Dsn1^{4A}, in which Aurora B phosphorylation sites are substituted with alanine (4A: S97A, S101A, S102A, and S111A), was expressed in AID-based CENP-T conditional knockdown CENP-C$^{\Delta 73}$/CENP-T^{WT} cells or CENP-C$^{\Delta 73}$/CENP-T$^{\Delta 161-216}$ cells. Cells were treated with IAA for 12 h, fixed, and stained with an anti-FLAG antibody. DNA was stained with DAPI. Scale bar, 10 μm.

(E) Quantification data of GFP-Dsn1 signals at kinetochores in mitotic cells shown in (D). Error bars show the mean ± SD; *p*-values were calculated by one-way ANOVA ($F(2,27) = 245.1$; $p < 0.0001$) followed by Tukey's test.

(F) Immunoprecipitation using anti-FLAG antibody in AID-based CENP-T conditional knockdown CENP-C$^{\Delta 73}$/CENP-T^{WT} cells or CENP-C$^{\Delta 73}$/CENP-T$^{\Delta 161-216}$ cells expressing GFP-Dsn1^{WT} or GFP-Dsn1^{4A}. Cells were cultured with IAA for 12 h and nocodazole was added for last 10 h before immunoprecipitation experiments. Immunoprecipitated samples were subjected to immunoblot analyses using anti-CENP-T, anti-FLAG, and anti-Dsn1 antibodies. Asterisk indicates nonspecific bands.

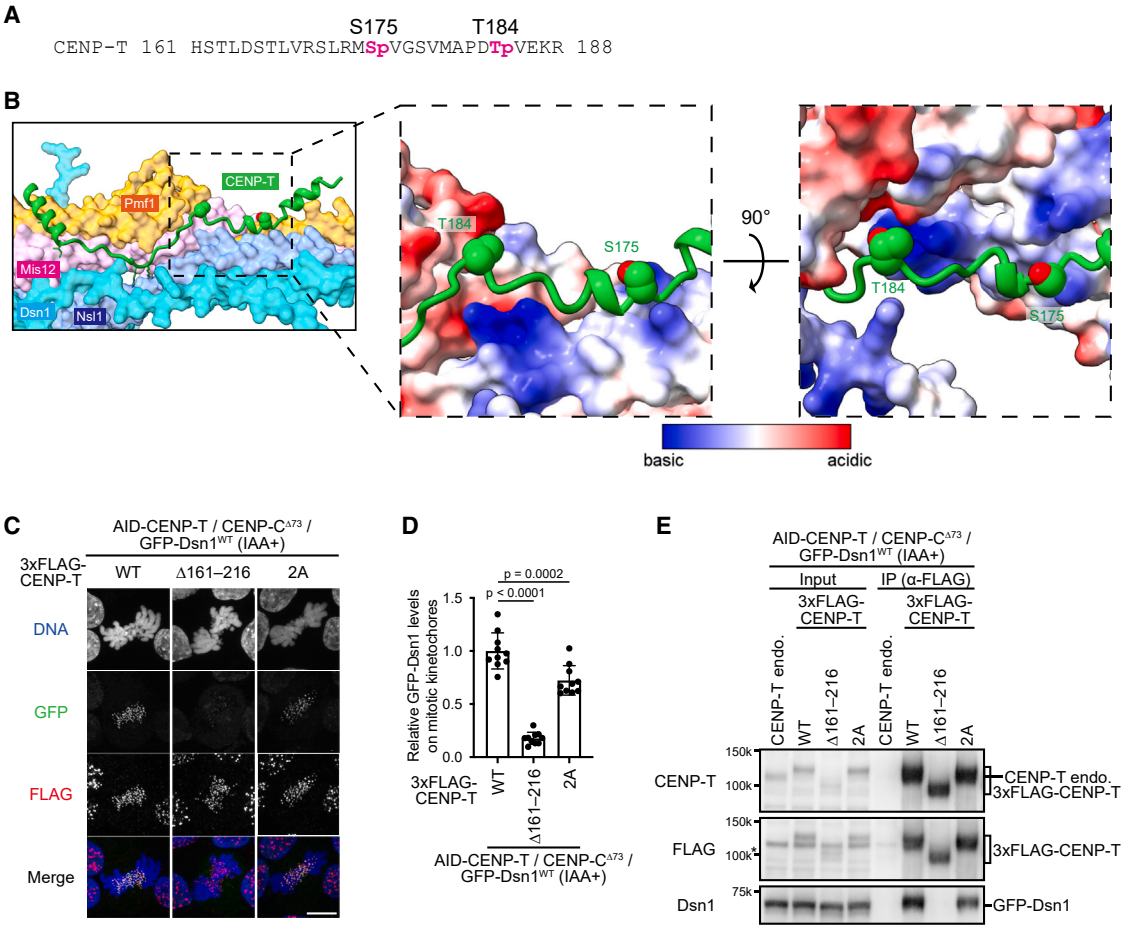

Figure 5. Phosphorylation of CENP-T regulates the chicken CENP-T-Mis12C interaction

(A) S175 and T184 of CENP-T are phosphorylated in mitotic DT40 cells based on phospho-mass spectrometry analysis.

(B) AlphaFold2 predicted structure of chicken Mis12C in complex with the Mis12C-binding domain of CENP-T. The transparent surface model of Mis12C is overlaid on a cartoon model. CENP-T is shown as a cartoon and models are color-coded as indicated in the figure. S175 and T184 of CENP-T are labeled. The dashed box shows the electrostatic potential of Mis12C mapped on the surface representation. CENP-T is also shown as a cartoon.

(C) Localization of GFP-Dsn1. 3xFLAG-CENP-T ^{WT}, 3xFLAG-CENP-T$^{\Delta161–216}$, or 3xFLAG-CENP-T^{2A} was expressed in AID-based CENP-T conditional knockdown CENP-C$^{\Delta73}$ cells. CENP-C$^{\Delta73}$/CENP-T^{WT}/Dsn1^{WT} cells and CENP-C$^{\Delta73}$/CENP-T$^{\Delta161–216}$/Dsn1^{WT} cells were also used in previous experiments. Cells were treated with IAA for 12 h, fixed, and stained with an anti-FLAG antibody. DNA was stained with DAPI. Scale bar, 10 μm.

(D) Quantification data of GFP-Dsn1 signals at kinetochores in mitotic cells shown in (C). Error bars show the mean ± SD; *p*-values were calculated by one-way ANOVA ($F(2,27) = 102.4$; $p < 0.0001$) followed by Tukey's test.

(E) Immunoprecipitation using anti-FLAG antibody in AID-based CENP-T conditional knockdown GFP-Dsn1/CENP-C$^{\Delta73}$ cells expressing 3xFLAG-CENP-T^{WT}, 3xFLAG-CENP-T$^{\Delta161–216}$, or 3xFLAG-CENP-T^{2A}. Cells were cultured with IAA for 12 h and nocodazole was added for last 10 h before immunoprecipitation experiments. Immunoprecipitated samples were subjected to immunoblot analyses using anti-CENP-T, anti-FLAG, and anti-Dsn1 antibodies. Asterisk indicates nonspecific bands.

of CENP-T and Dsn1 double mutations on Mis12C localization at the kinetochores. GFP-Dsn1 levels at kinetochores in CENP-C$^{\Delta73}$/CENP-T^{WT}/Dsn1^{4A} and CENP-C$^{\Delta73}$/CENP-T^{2A}/Dsn1^{WT} cells were reduced by ~65% and ~70%, respectively, compared to those in CENP-C$^{\Delta73}$/CENP-T^{WT}/Dsn1^{WT} cells (Figures 6A and 6B). However, Dsn1 levels at kinetochores in CENP-C$^{\Delta73}$/CENP-T^{2A}/Dsn1^{4A} cells were reduced to approximately 30% of those in CENP-C$^{\Delta73}$/CENP-T^{WT}/Dsn1^{WT} cells (Figures 6A and 6B and Table S1), indicating an additive reduction effect of Dsn1^{4A} and CENP-T^{2A} on Mis12C levels at kinetochores. This additive effect was confirmed using co-immunoprecipitation. GFP-Dsn1 levels were further decreased in the CENP-T-immunoprecipitated fraction of CENP-C$^{\Delta73}$/CENP-T^{2A}/Dsn1^{4A} cells, compared to those in the CENP-C$^{\Delta73}$/CENP-T^{WT}/Dsn1^{4A} or CENP-C$^{\Delta73}$/CENP-T^{2A}/Dsn1^{WT} cells (Figure 6C). Consistent with these results, CENP-C$^{\Delta73}$/CENP-T^{2A}/Dsn1^{4A} cells showed a growth delay (Figure S7B). Then, we found that the M phase proportion in CENP-C$^{\Delta73}$/CENP-T^{2A}/Dsn1^{4A} cells was significantly increased compared to that in CENP-C$^{\Delta73}$/CENP-T^{WT}/Dsn1^{WT}, CENP-C$^{\Delta73}$/CENP-T^{WT}/Dsn1^{4A}, or CENP-C$^{\Delta73}$/CENP-T^{2A}/Dsn1^{WT} cells (Figure 6D). We also assessed the sensitivity of these cells to low doses of nocodazole, inhibitor

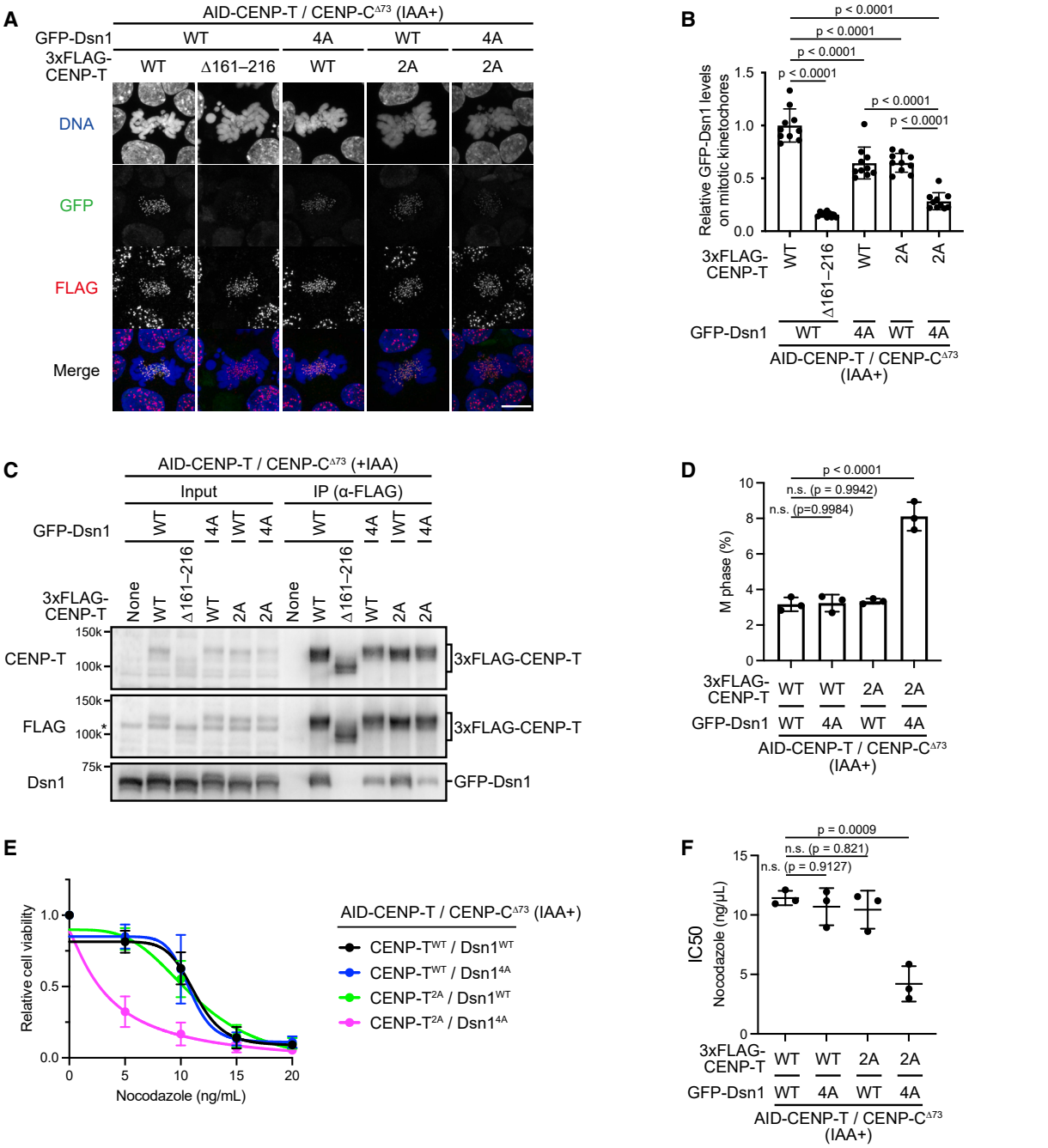

Figure 6. Dual phosphorylation of Dsn1 and CENP-T ensures the timely and robust chicken CENP-T-Mis12C interaction

(A) Localization of GFP-Dsn1: 3xFLAG-CENP-T ^{WT}, 3xFLAG-CENP-T$^{\Delta 161–216}$, or 3xFLAG-CENP-T^{2A} was expressed in AID-based CENP-T conditional knockdown CENP-C$^{\Delta 73}$/Dsn1^{WT} cells or CENP-C$^{\Delta 73}$/Dsn1^{4A} cells. CENP-C$^{\Delta 73}$/CENP-T^{WT}/Dsn1^{WT} cells, CENP-C$^{\Delta 73}$/CENP-T$^{\Delta 161–216}$/Dsn1^{WT} cells, CENP-C$^{\Delta 73}$/CENP-T^{WT}/Dsn1^{4A} cells, and CENP-C$^{\Delta 73}$/CENP-T^{2A}/Dsn1^{WT} cells were also used in previous experiments. Cells were treated with IAA for 12 h, fixed, and stained with an anti-FLAG antibody. DNA was stained with DAPI. Scale bar, 10 μm.

(B) Quantification of GFP-Dsn1 signals at kinetochores in mitotic cells shown in (A). Error bars show the mean ± SD; *p*-values were calculated by one-way ANOVA ($F(4,45) = 89.33$; $p < 0.0001$) followed by Tukey's test.

(C) Immunoprecipitation using anti-FLAG antibody in AID-based CENP-T conditional knockdown CENP-C$^{\Delta 73}$/Dsn1^{WT} cells or CENP-C$^{\Delta 73}$/Dsn1^{4A} cells expressing 3xFLAG-CENP-T^{WT}, 3xFLAG-CENP-T$^{\Delta 161–216}$, or 3xFLAG-CENP-T^{2A}. Cells were cultured with IAA for 12 h and nocodazole was added for last 10 h before immunoprecipitation experiments. Immunoprecipitated samples were subjected to immunoblot analyses using anti-CENP-T, anti-FLAG, and anti-Dsn1 antibodies. Asterisk indicates nonspecific bands.

(legend continued on next page)

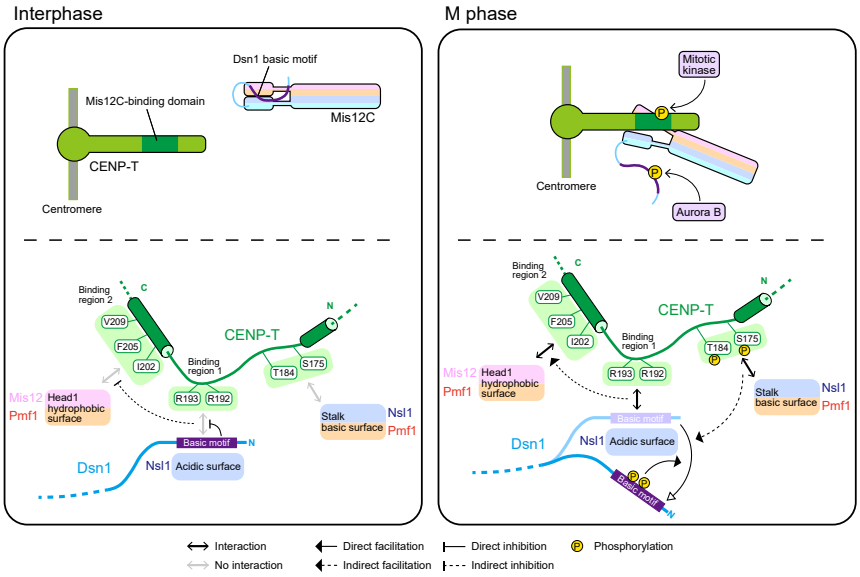

Figure 7. A model of the regulatory mechanism of the CENP-T-Mis12C interaction during interphase and M phase

A model of the regulatory mechanism of the CENP-T-Mis12C interaction. In interphase, the Dsn1 basic motif masks the Nsl1 acidic surface, inhibiting the interaction between binding region 1 of CENP-T and the Nsl1 acidic surface of Mis12C. This inhibition leads to the inhibition of the interaction between binding region 2 of CENP-T and the Head1 hydrophobic surface of Mis12C. Since CENP-T is not phosphorylated in interphase, S175 and T184 of CENP-T do not interact with the stalk basic surface of Mis12C. In M phase, the Dsn1 basic motif is precluded from the Nsl1 acidic surface by the CENP-T and Dsn1 dual phosphoregulation. Phosphorylation of the Dsn1 basic motif by Aurora B precludes the mask by inhibiting the basic motif binding to the Nsl1 acidic surface. Phosphorylated residues of CENP-T may interact with Mis12C basic surface, helping to preclude the mask by increasing the overall affinity of the CENP-T-Mis12C interaction. By coordination of CENP-T and Dsn1 dual phosphorylation, the Nsl1 acidic surface associates with binding region 1 of CENP-T.

of microtubule polymerization. While the 5 ng/mL nocodazole treatment did not affect the cell viability of CENP-$C^{\Delta73}$/CENP-T^{WT}/$Dsn1^{WT}$, CENP-$C^{\Delta73}$/CENP-T^{WT}/$Dsn1^{4A}$, or CENP-$C^{\Delta73}$/CENP-T^{2A}/$Dsn1^{WT}$ cells, the cell viability of CENP-$C^{\Delta73}$/CENP-T^{2A}/$Dsn1^{4A}$ cells was decreased by the treatment with the same concentration of nocodazole (Figures 6E and 6F), suggesting that CENP-$C^{\Delta73}$/CENP-T^{2A}/$Dsn1^{4A}$ cells are sensitive to the low-dose nocodazole treatment possibly due to the reduction in the kinetochore-localized Mis12C levels. Based on these results, phosphorylation of both Dsn1 and CENP-T is important for timely and stable CENP-T-Mis12C interaction during mitosis, and this regulatory mechanism is critical for mitotic progression and proliferation of CENP-$C^{\Delta73}$ cells.

DISCUSSION

In this study, we demonstrated that CENP-T binds to Mis12C mainly via two interaction regions (binding regions 1 and 2), and each of them is important for Mis12C binding. In addition, a third region of CENP-T containing residues S175 and T184 seems to contribute to the binding to Mis12C when CENP-T is phosphorylated. These interactions are cooperatively regulated by dual phosphorylation of Dsn1 and CENP-T, ensuring timely and robust CENP-T-Mis12C interactions during mitosis (Figure 7; see below).

The two Mis12C-binding regions of CENP-T are important for the CENP-T-Mis12C interaction. The binding region 2 alone does not seem to be sufficient for binding as evidenced by the ability of the Dsn1 basic motif that competes only with the binding region 1 to completely abolish the interaction with CENP-T in interphase. This mechanism explains complete inhibition of the CENP-T-Mis12C interaction in interphase (Interphase; Figure 7). In addition, Mis12C containing the Dsn1 mutant lacking the basic motif ($Dsn1^{\Delta93–114}$) binds to CENP-T in interphase cells, suggesting that the deletion of the Dsn1 basic motif facilitates the interactions via two interaction surfaces. Therefore, we propose that phosphorylation of the Dsn1 basic motif by Aurora B can facilitate the interactions via two interaction surfaces simultaneously for timely CENP-T-Mis12C interaction during mitosis (M phase; Figure 7).

A highlight of this paper is CENP-T and Dsn1 dual phosphoregulation for the CENP-T-Mis12C interaction during mitosis. Although each phosphorylation can recruit sufficient levels of Mis12C at kinetochores for cell proliferation, both mutations for CENP-T and Dsn1 showed additional reduction of Mis12C and caused mitotic defects. How are these dual phosphoregulation related each other? Mis12C levels at kinetochores were reduced in CENP-$C^{\Delta73}$/$Dsn1^{4A}$ cells, but these are still higher than those in CENP-$C^{\Delta73}$/CENP-T^{RR-AA} cells that have mutations in binding region 1 of CENP-T, which is important for Mis12C-binding. This

(D) The ratio of M phase population in indicated cell lines. Cells were treated with IAA for 12 h and fixed. DNA was stained with DAPI. Populations for M phase and interphase were counted in each cell line, and the ratio of M phase cells was calculated. The experiments were repeated three times, and error bars show the mean of the three replicates ±SD; *p*-values were calculated using one-way ANOVA ($F(3,8) = 67.87$; $p < 0.0001$) followed by Tukey's test.

(E) Viability of cells treated with various nocodazole concentrations in indicated cell lines. 3xFLAG-CENP-T^{WT} or 3xFLAG-CENP-T^{2A} was expressed in AID-based CENP-T conditional knockdown CENP-$C^{\Delta73}$/$Dsn1^{WT}$ cells or CENP-$C^{\Delta73}$/$Dsn1^{4A}$ cells, treated with IAA for 12 h, and added nocodazole. Cell viability was measured 24 h after nocodazole addition. The experiments were repeated three times, and error bars show the mean of the three replicates ±SD.

(F) Half-maximal inhibitory concentration (IC50) of nocodazole calculated using the data shown in (E). The experiments were repeated three times, and error bars show the mean of the three replicates ±SD; *p*-values were calculated by one-way ANOVA ($F(3,8) = 17.76$; $p = 0.0007$) followed by Tukey's test.

result suggests that there is a state of Mis12C in which the Dsn1 basic motif is precluded, even if Aurora B phosphorylation sites of Dsn1 are mutated in CENP-C$^{\Delta 73}$/Dsn1^{4A} cells. The CENP-T phosphorylation sites may directly bind to Mis12C, as AlphaFold3 predicted that phosphorylated S175 and T184 of CENP-T are close to the basic region of Mis12C. We propose that the CENP-T phosphorylation contributes to the exclusion of the Dsn1 basic motif mask by increasing the overall affinity of the CENP-T-Mis12C interaction (Figures 7 and S6F). Our results suggest that phosphorylation of CENP-T and Dsn1 can coordinately preclude the Dsn1 basic motif mask. Thus, in our model, both CENP-T and Dsn1 phosphorylation may contribute to the CENP-T-Mis12C interaction in early mitosis (Figure S7D). The Dsn1 mask is released by co-ordination of Dsn1 and CENP-T phosphorylation allowing CENP-T-binding region 1 to stably bind to Nsl1 of Mis12C, which leads to the hydrophobic interaction via CENP-T-binding region 2 with Mis12C (Figures 7 and S7D).

Interestingly, Mis12C localization to interphase centromeres depends on CENP-C (Figure 1). For the CENP-C-Mis12C interaction during mitosis, the involvement of phosphoregulation of Dsn1 has been well studied.[18,26,28,31,32] Our AlphaFold2 prediction suggests that CENP-C is likely to bind to Mis12C in the auto-inhibited state (Figures S1G–S1K) during interphase, independent of Dsn1 phosphoregulation. This finding supports the results of a previous *in vitro* binding assay showing that CENP-C binds to Mis12C in the auto-inhibited state.[26] However, the significance of interphase Mis12C localization at kinetochores via CENP-C remains unclear. A recent study demonstrated that Mis12C constitutively localizes to the centromeres in mouse germ cells expressing the Dsn1 isoform, which lacks the basic motif.[34] They proposed that the continuous kinetochore localization of Mis12C might be important for stable KMN network assembly because germ cells immediately enter meiosis II after meiosis I without DNA replication. Similarly, interphase Mis12C localization at kinetochores via CENP-C may be important for timely KMN network assembly for the subsequent mitosis in cells.

In both CENP-C- and CENP-T-pathways, phosphorylation by Aurora B facilitates the CENP-C- or CENP-T-Mis12C interaction. Aurora B also phosphorylates Ndc80C on kinetochores on unaligned chromosomes to correct erroneous microtubule attachments and phosphorylation levels by Aurora B is decreased at kinetochores on aligned chromosomes.[35] However, even at Aurora B less-kinetochores on aligned chromosomes, Mis12C localizes at kinetochores. Therefore, we propose that the CENP-C- or CENP-T-Mis12C interaction independent of Aurora B-mediated regulations is important to maintain Mis12 C at kinetochores on aligned chromosomes for proper mitotic progression.

Recent structural analyses of the KMN network or CCAN using *in vitro* reconstitution have provided valuable insights into the mechanism underlying kinetochore assembly.[9,10,26,31] However, it is still largely unknown how kinetochore components play a role in mitotic progression. Therefore, it is critical to evaluate the significance of the binding surfaces between kinetochore components, which have been clarified by structural analyses. Some kinetochore components have similar functions and simultaneously recruit the same proteins,[14,15,17,36] making it difficult to investigate the significance of each interaction in cells. In this study, using chicken DT40 cells lacking the CENP-C-Mis12C interaction, we clearly elucidated the significance of the interaction surfaces and phosphoregulation for the CENP-T-Mis12C interaction in cells. This knowledge provides important insights into how functional kinetochores are established in cells.

Limitations of the study

We propose the interaction surfaces and phosphoregulation for the CENP-T-Mis12C interaction, based on structure prediction and cell biological and biochemical experiments. However, we did not obtain experimental structure data for the CENP-T-Mis12C interaction. We found that the CENP-T-Mis12C interaction is dynamic in cells, and it is possible that there are additional regulations for the interaction. Further structural studies would uncover unsolved mechanisms for the CENP-T-Mis12C interaction.

RESOURCE AVAILABILITY

Lead contact

Further information and any requests should be directed to and will be fulfilled by the lead contact, Tatsuo Fukagawa (fukagawa.tatsuo.fbs@osaka-u.ac.jp).

Materials availability

This study did not generate new unique reagents. Plasmids and cell lines generated in this study are available upon request. Any additional analysis information for this work is available by request to the lead contact.

Data and code availability

- All data reported in this paper will be shared by the lead contact upon request.
- This article does not report original code.
- Any additional information required to reanalyze the data reported in this paper is available from the lead contact upon request.

ACKNOWLEDGMENTS

The authors are very grateful to Y. Kubota and R. Fukuoka for their technical assistance. This work was supported by CREST of JST (21460153), JSPS KAKENHI Grant Numbers 20H05389, 21H05752, 22H00408, 22H04692, and 24H02281 to T.F., JSPS KAKENHI Grant Numbers 22K20630 and 23K14180 to Y.T., JSPS KAKENHI Grant Numbers 21H02461, 22H04672, and 24K02005, Takeda Science Foundation and Daiichi Sankyo Foundation of Life Science to M.H., JSPS KAKENHI Grant Number 24K09340 to M.A..

AUTHOR CONTRIBUTIONS

Conceptualization: Y.T. and T.F.; Investigation: Y.T., M.H., R.N., and M.A.; Formal analysis: Y.T. and R.N.; Resources: M.H.; Data curation: Y.T.; Writing – original draft: T.F.; Writing – review and editing: T.F. and Y.T.; Project administration: T.F.; Funding acquisition: T.F., Y.T., M.H., and M.A.

DECLARATION OF INTERESTS

The authors declare no competing interests.

STAR★METHODS

Detailed methods are provided in the online version of this paper and include the following:

- KEY RESOURCES TABLE
- EXPERIMENTAL MODEL AND STUDY PARTICIPANT DETAILS

SUPPLEMENTAL INFORMATION

Supplemental information can be found online at https://doi.org/10.1016/j.isci.2024.111295.

Received: June 12, 2024
Revised: July 10, 2024
Accepted: October 29, 2024
Published: November 1, 2024

REFERENCES

1. Fukagawa, T., and Earnshaw, W.C. (2014). The centromere: chromatin foundation for the kinetochore machinery. Dev. Cell *30*, 496–508. https://doi.org/10.1016/j.devcel.2014.08.016.
2. McKinley, K.L., and Cheeseman, I.M. (2016). The molecular basis for centromere identity and function. Nat. Rev. Mol. Cell Biol. *17*, 16–29. https://doi.org/10.1038/nrm.2015.5.
3. Hara, M., and Fukagawa, T. (2017). Critical Foundation of the Kinetochore: The Constitutive Centromere-Associated Network (CCAN). Prog. Mol. Subcell. Biol. *56*, 29–57. https://doi.org/10.1007/978-3-319-58592-5_2.
4. Hara, M., and Fukagawa, T. (2018). Kinetochore assembly and disassembly during mitotic entry and exit. Curr. Opin. Cell Biol. *52*, 73–81. https://doi.org/10.1016/j.ceb.2018.02.005.
5. Hori, T., Amano, M., Suzuki, A., Backer, C.B., Welburn, J.P., Dong, Y., McEwen, B.F., Shang, W.H., Suzuki, E., Okawa, K., et al. (2008). CCAN makes multiple contacts with centromeric DNA to provide distinct pathways to the outer kinetochore. Cell *135*, 1039–1052. https://doi.org/10.1016/j.cell.2008.10.019.
6. Nagpal, H., and Fukagawa, T. (2016). Kinetochore assembly and function through the cell cycle. Chromosoma *125*, 645–659. https://doi.org/10.1007/s00412-016-0608-3.
7. Pesenti, M.E., Weir, J.R., and Musacchio, A. (2016). Progress in the structural and functional characterization of kinetochores. Curr. Opin. Struct. Biol. *37*, 152–163. https://doi.org/10.1016/j.sbi.2016.03.003.
8. Musacchio, A., and Desai, A. (2017). A Molecular View of Kinetochore Assembly and Function. Biology *6*, 5. https://doi.org/10.3390/biology6010005.
9. Yatskevich, S., Muir, K.W., Bellini, D., Zhang, Z., Yang, J., Tischer, T., Predin, M., Dendooven, T., McLaughlin, S.H., and Barford, D. (2022). Structure of the human inner kinetochore bound to a centromeric CENP-A nucleosome. Science *376*, 844–852. https://doi.org/10.1126/science.abn3810.
10. Pesenti, M.E., Raisch, T., Conti, D., Walstein, K., Hoffmann, I., Vogt, D., Prumbaum, D., Vetter, I.R., Raunser, S., and Musacchio, A. (2022). Structure of the human inner kinetochore CCAN complex and its significance for human centromere organization. Mol. Cell *82*, 2113–2131.e8. https://doi.org/10.1016/j.molcel.2022.04.027.
11. Cheeseman, I.M., Chappie, J.S., Wilson-Kubalek, E.M., and Desai, A. (2006). The conserved KMN network constitutes the core microtubule-binding site of the kinetochore. Cell *127*, 983–997. https://doi.org/10.1016/j.cell.2006.09.039.
12. DeLuca, J.G., Gall, W.E., Ciferri, C., Cimini, D., Musacchio, A., and Salmon, E.D. (2006). Kinetochore microtubule dynamics and attachment stability are regulated by Hec1. Cell *127*, 969–982. https://doi.org/10.1016/j.cell.2006.09.047.
13. Alushin, G.M., Ramey, V.H., Pasqualato, S., Ball, D.A., Grigorieff, N., Musacchio, A., and Nogales, E. (2010). The Ndc80 kinetochore complex forms oligomeric arrays along microtubules. Nature *467*, 805–810. https://doi.org/10.1038/nature09423.
14. Hori, T., Shang, W.H., Takeuchi, K., and Fukagawa, T. (2013). The CCAN recruits CENP-A to the centromere and forms the structural core for kinetochore assembly. J. Cell Biol. *200*, 45–60. https://doi.org/10.1083/jcb.201210106.
15. Nishino, T., Rago, F., Hori, T., Tomii, K., Cheeseman, I.M., and Fukagawa, T. (2013). CENP-T provides a structural platform for outer kinetochore assembly. EMBO J. *32*, 424–436. https://doi.org/10.1038/emboj.2012.348.
16. Kim, S., and Yu, H. (2015). Multiple assembly mechanisms anchor the KMN spindle checkpoint platform at human mitotic kinetochores. J. Cell Biol. *208*, 181–196. https://doi.org/10.1083/jcb.201407074.
17. Rago, F., Gascoigne, K.E., and Cheeseman, I.M. (2015). Distinct organization and regulation of the outer kinetochore KMN network downstream of CENP-C and CENP-T. Curr. Biol. *25*, 671–677. https://doi.org/10.1016/j.cub.2015.01.059.
18. Hara, M., Ariyoshi, M., Okumura, E.I., Hori, T., and Fukagawa, T. (2018). Multiple phosphorylations control recruitment of the KMN network onto kinetochores. Nat. Cell Biol. *20*, 1378–1388. https://doi.org/10.1038/s41556-018-0230-0.
19. Sridhar, S., and Fukagawa, T. (2022). Kinetochore Architecture Employs Diverse Linker Strategies Across Evolution. Front. Cell Dev. Biol. *10*, 862637. https://doi.org/10.3389/fcell.2022.862637.
20. Ariyoshi, M., and Fukagawa, T. (2023). An updated view of the kinetochore architecture. Trends Genet. *39*, 941–953. https://doi.org/10.1016/j.tig.2023.09.003.
21. Petrovic, A., Pasqualato, S., Dube, P., Krenn, V., Santaguida, S., Cittaro, D., Monzani, S., Massimiliano, L., Keller, J., Tarricone, A., et al. (2010). The MIS12 complex is a protein interaction hub for outer kinetochore assembly. J. Cell Biol. *190*, 835–852. https://doi.org/10.1083/jcb.201002070.
22. Huis In 't Veld, P.J., Jeganathan, S., Petrovic, A., Singh, P., John, J., Krenn, V., Weissmann, F., Bange, T., and Musacchio, A. (2016). Molecular basis of outer kinetochore assembly on CENP-T. Elife *5*, e21007. https://doi.org/10.7554/eLife.21007.
23. Suzuki, A., Badger, B.L., and Salmon, E.D. (2015). A quantitative description of Ndc80 complex linkage to human kinetochores. Nat. Commun. *6*, 8161. https://doi.org/10.1038/ncomms9161.
24. Takenoshita, Y., Hara, M., and Fukagawa, T. (2022). Recruitment of two Ndc80 complexes via the CENP-T pathway is sufficient for kinetochore functions. Nat. Commun. *13*, 851. https://doi.org/10.1038/s41467-022-28403-8.
25. Walstein, K., Petrovic, A., Pan, D., Hagemeier, B., Vogt, D., Vetter, I.R., and Musacchio, A. (2021). Assembly principles and stoichiometry of a complete human kinetochore module. Sci. Adv. *7*, eabg1037. https://doi.org/10.1126/sciadv.abg1037.
26. Yatskevich, S., Yang, J., Bellini, D., Zhang, Z., and Barford, D. (2024). Structure of the human outer kinetochore KMN network complex. Nat. Struct. Mol. Biol. *31*, 874–883. https://doi.org/10.1038/s41594-024-01249-y.
27. Gascoigne, K.E., Takeuchi, K., Suzuki, A., Hori, T., Fukagawa, T., and Cheeseman, I.M. (2011). Induced ectopic kinetochore assembly bypasses

the requirement for CENP-A nucleosomes. Cell *145*, 410–422. https://doi.org/10.1016/j.cell.2011.03.031.

28. Petrovic, A., Keller, J., Liu, Y., Overlack, K., John, J., Dimitrova, Y.N., Jenni, S., van Gerwen, S., Stege, P., Wohlgemuth, S., et al. (2016). Structure of the MIS12 Complex and Molecular Basis of Its Interaction with CENP-C at Human Kinetochores. Cell *167*, 1028–1040.e15. https://doi.org/10.1016/j.cell.2016.10.005.
29. Fukagawa, T., and Brown, W.R. (1997). Efficient conditional mutation of the vertebrate CENP-C gene. Hum. Mol. Genet. *6*, 2301–2308.
30. Fukagawa, T., Pendon, C., Morris, J., and Brown, W. (1999). CENP-C is necessary but not sufficient to induce formation of a functional centromere. EMBO J. *18*, 4196–4209. https://doi.org/10.1093/emboj/18.15.4196.
31. Polley, S., Raisch, T., Ghetti, S., Körner, M., Terbeck, M., Gräter, F., Raunser, S., Aponte-Santamaría, C., Vetter, I.R., and Musacchio, A. (2024). Structure of the human KMN complex and implications for regulation of its assembly. Nat. Struct. Mol. Biol. *31*, 861–873. https://doi.org/10.1038/s41594-024-01230-9.
32. Dimitrova, Y.N., Jenni, S., Valverde, R., Khin, Y., and Harrison, S.C. (2016). Structure of the MIND Complex Defines a Regulatory Focus for Yeast Kinetochore Assembly. Cell *167*, 1014–1027.e12. https://doi.org/10.1016/j.cell.2016.10.011.
33. Welburn, J.P.I., Vleugel, M., Liu, D., Yates, J.R., 3rd, Lampson, M.A., Fukagawa, T., and Cheeseman, I.M. (2010). Aurora B phosphorylates spatially distinct targets to differentially regulate the kinetochore-microtubule interface. Mol. Cell *38*, 383–392. https://doi.org/10.1016/j.molcel.2010.02.034.
34. Ly, J., Blengini, C.S., Cady, S.L., Schindler, K., and Cheeseman, I.M. (2024). A conserved germline-specific Dsn1 alternative splice isoform supports oocyte and embryo development. Curr. Biol. *34*, 4307–4317. https://doi.org/10.1016/j.cub.2024.07.089.
35. Salimian, K.J., Ballister, E.R., Smoak, E.M., Wood, S., Panchenko, T., Lampson, M.A., and Black, B.E. (2011). Feedback control in sensing chromosome biorientation by the Aurora B kinase. Curr. Biol. *21*, 1158–1165. https://doi.org/10.1016/j.cub.2011.06.015.
36. Nguyen, A.L., Fadel, M.D., and Cheeseman, I.M. (2021). Differential requirements for the CENP-O complex reveal parallel PLK1 kinetochore recruitment pathways. Mol. Biol. Cell *32*, 712–721. https://doi.org/10.1091/mbc.E20-11-0751.
37. Regnier, V., Vagnarelli, P., Fukagawa, T., Zerjal, T., Burns, E., Trouche, D., Earnshaw, W., and Brown, W. (2005). CENP-A is required for accurate chromosome segregation and sustained kinetochore association of BubR1. Mol. Cell. Biol. *25*, 3967–3981. https://doi.org/10.1128/MCB.25.10.3967-3981.2005.
38. Buerstedde, J.M., Reynaud, C.A., Humphries, E.H., Olson, W., Ewert, D.L., and Weill, J.C. (1990). Light chain gene conversion continues at high rate in an ALV-induced cell line. EMBO J. *9*, 921–927.
39. Cong, L., Ran, F.A., Cox, D., Lin, S., Barretto, R., Habib, N., Hsu, P.D., Wu, X., Jiang, W., Marraffini, L.A., and Zhang, F. (2013). Multiplex genome engineering using CRISPR/Cas systems. Science *339*, 819–823. https://doi.org/10.1126/science.1231143.
40. Cao, J., Hori, T., Ariyoshi, M., and Fukagawa, T. (2024). Artificial tethering of constitutive centromere-associated network proteins induces CENP-A deposition without Knl2 in DT40 cells. J. Cell Sci. *137*, jcs261639. https://doi.org/10.1242/jcs.261639.
41. Nishimura, K., Yamada, R., Hagihara, S., Iwasaki, R., Uchida, N., Kamura, T., Takahashi, K., Torii, K.U., and Fukagawa, T. (2020). A super-sensitive auxin-inducible degron system with an engineered auxin-TIR1 pair. Nucleic Acids Res. *48*, e108. https://doi.org/10.1093/nar/gkaa748.
42. Schindelin, J., Arganda-Carreras, I., Frise, E., Kaynig, V., Longair, M., Pietzsch, T., Preibisch, S., Rueden, C., Saalfeld, S., Schmid, B., et al. (2012). Fiji: an open-source platform for biological-image analysis. Nat. Methods *9*, 676–682. https://doi.org/10.1038/nmeth.2019.
43. Mirdita, M., Schütze, K., Moriwaki, Y., Heo, L., Ovchinnikov, S., and Steinegger, M. (2022). ColabFold: making protein folding accessible to all. Nat. Methods *19*, 679–682. https://doi.org/10.1038/s41592-022-01488-1.
44. Hara, M., Ariyoshi, M., Sano, T., Nozawa, R.S., Shinkai, S., Onami, S., Jansen, I., Hirota, T., and Fukagawa, T. (2023). Centromere/kinetochore is assembled through CENP-C oligomerization. Mol. Cell *83*, 2188–2205.e13. https://doi.org/10.1016/j.molcel.2023.05.023.
45. Hori, T., Cao, J., Nishimura, K., Ariyoshi, M., Arimura, Y., Kurumizaka, H., and Fukagawa, T. (2020). Essentiality of CENP-A Depends on Its Binding Mode to HJURP. Cell Rep. *33*, 108388. https://doi.org/10.1016/j.celrep.2020.108388.
46. Hughes, C.S., Moggridge, S., Müller, T., Sorensen, P.H., Morin, G.B., and Krijgsveld, J. (2019). Single-pot, solid-phase-enhanced sample preparation for proteomics experiments. Nat. Protoc. *14*, 68–85. https://doi.org/10.1038/s41596-018-0082-x.

STAR★METHODS

KEY RESOURCES TABLE

REAGENT or RESOURCE	SOURCE	IDENTIFIER
Antibodies		
Mouse monoclonal anti-α-tubulin	Sigma	Cat#T9026; RRID: AB_477593
Mouse monoclonal anti-FLAG	Sigma	Cat#F1804; RRID: AB_262044
Rabbit anti-chicken CENP-C	Takenoshita et al.[24]	RRID: AB_3665351
Rabbit anti-chicken CENP-T	Hori et al.[5]	RRID: AB_2665551
Rabbit anti-chicken CENP-A	Regnier et al.[37]	RRID: AB_2665547
Rabbit anti-chicken Dsn1	Hara et al.[18]	RRID: AB_2756344
Rat monoclonal anti-RFP	Chromotek	Cat#5F8; RRID: AB_2336064
HRP-conjugated anti-Rabbit IgG	Jackson ImmunoResearch	Cat#: 111-035-144; RRID: AB_2307391
HRP-conjugated anti-mouse IgG	Jackson ImmunoResearch	Cat#: 115-035-003; RRID: AB_10015289
HRP-conjugated anti-Rat IgG	Jackson ImmunoResearch	Cat#112-035-003; RRID: AB_2338128
Cy3-conjugated mouse anti-rabbit IgG	Jackson ImmunoResearch	Cat#: 211-165-109; RRID: AB_233915
Cy3-conjugated goat anti-mouse IgG	Jackson ImmunoResearch	Cat#: 115-165-146; RRID: AB_2338690
Bacterial and virus strains		
E.coli. DH5α	TOYOBO	Cat#: DNA-903
Chemicals, peptides, and recombinant proteins		
Penicillin-Streptomycin	Thermo Fisher	Cat#15140-122
3-Indole acetic acid (IAA)	Wako	Cat#090-07123
In-Fusion Snap Assembly Master Mix	Takara Bio	Cat#639648
puromycin	Takara	Cat#Z1305N
G418	Santa Cruz Biotechnology	Cat#SC-29065B
Blasticidin S hydrochloride	Kaken Pharmaceutical	Cat#KK-400
L-Histidinol dihydrochloride	Sigma	Cat#H6647
Zeocin	Invitrogen	Cat#45-0430
mycophenolic acid	Tokyo Chemical Industry	Cat#M2216
xanthine	Sigma	Cat#X4002
ECL Prime Western Blotting Detection Reagent	Cytiva	Cat#RPN2232
Nocodazole	Sigma	Cat#M1404
Signal Enhancer Hikari	Nacalai tesque	Cat#02270-81
DAPI	Roche	Cat#10236276001
VECTASHIELD Mounting Medium	Vector Laboratories	Cat#H-1000
cOmplete™, EDTA-free Protease Inhibitor Cocktail	Roche	Cat#5056489001
PhosSTOP™	Roche	Cat#4906845001
TurboNuclease	Accelagen	Cat# N0103P
MG132	Sigma	Cat#C2211
Critical commercial assays		
RealTime-Glo MT Cell Viability Assay	Promega	Cat#G9711
Experimental models: Cell lines		
CL18 (DT40 WT) cells	Buerstedde et al.[38]	N/A
CL18 / GFP-Dsn1^{WT} cells	Takenoshita et al.[24]	N/A

(*Continued on next page*)

Continued

REAGENT or RESOURCE	SOURCE	IDENTIFIER
CL18 / CENP-C$^{\Delta 73}$ / GFP-Dsn1^{WT} cells	Takenoshita et al.[24]	N/A
CL18 / CENP-C$^{\Delta 73}$ / GFP-Dsn1$^{\Delta 93–114}$ cells	This paper	N/A
CL18 / CENP-C$^{\Delta 73}$ / 3xFLAG-CENP-T^{WT} / spot-Dsn1^{WT} cells	This paper	N/A
CL18 / CENP-C$^{\Delta 73}$ / AID-CENP-T / GFP-Dsn1^{WT} cells	This paper	N/A
CL18 / CENP-C$^{\Delta 73}$ / AID-CENP-T / GFP-Dsn1^{WT} / 3xFLAG-CENP-T^{WT} cells	This paper	N/A
CL18 / CENP-C$^{\Delta 73}$ / AID-CENP-T / GFP-Dsn1^{WT} / 3xFLAG-CENP-T$^{\Delta 161–216}$ cells	This paper	N/A
CL18 / CENP-C$^{\Delta 73}$ / AID-CENP-T / GFP-Dsn1^{WT} / 3xFLAG-CENP-T$^{IFV\text{-}RRR}$ cells	This paper	N/A
CL18 / CENP-C$^{\Delta 73}$ / AID-CENP-T / GFP-Dsn1^{WT} / 3xFLAG-CENP-T $^{RR\text{-}AA}$ cells	This paper	N/A
CL18 / CENP-C$^{\Delta 73}$ / AID-CENP-T / GFP-Dsn1^{WT} / 3xFLAG-CENP-T^{2A} cells	This paper	N/A
CL18 / CENP-C$^{\Delta 73}$ / AID-CENP-T / GFP-Dsn1^{4A} / 3xFLAG-CENP-T^{WT} cells	This paper	N/A
CL18 / CENP-C$^{\Delta 73}$ / AID-CENP-T / GFP-Dsn1^{4A} / 3xFLAG-CENP-T^{2A} cells	This paper	N/A
Oligonucleotides		
F1: 5'-ATTCCGCACGCTTCAAAAGC-3'	Takenoshita et al.[24]	N/A
R1: 5'-CTCTCCAGGGTCAGGTTCTGTG-3'	Takenoshita et al.[24]	N/A
F2: 5'-CTGAATGGATGTTTCTGACCTGCCTTG-3'	This study	N/A
R2: 5'-CGGCGACGATGAAAATAAAACTAAGGCTG-3'	This study	N/A
F3: 5'-GAAAGTCCCTATTGGCGTTAC-3'	Takenoshita et al.[24]	N/A
R3: 5'-CTGTGATGGCACCAGACACTG-3'	This study	N/A
F4: 5'-GGCGTAGGCCAGAGGTGTCTCC-3'	Takenoshita et al.[24]	N/A
R4: 5'-AGGCTCTGGTCGAGCATCTTCTG-3'	Takenoshita et al.[24]	N/A
F5: 5'-GCCGATCATAATCAGCCATACC-3'	Takenoshita et al.[24]	N/A
R5: 5'-GAACTGTCTGAAGTGCTAGAGG-3'	Takenoshita et al.[24]	N/A
R6: 5'-TAAACGCCCTCAAGGAGCAAG-3'	This study	N/A
Recombinant DNA		
pX330	Cong et al.[39]	Addgene plasmid #42230
pX330_ggDsn1	Takenoshita et al.[24]	N/A
pX335_ggPGK	Cao et al.[40]	N/A
pX330_ggCENP-T	This paper	N/A
pBS_Dsn1-N KI_GFP-Dsn1^{WT}_PuroR	Takenoshita et al.[24]	N/A
pBS_Dsn1-N KI_GFP-Dsn1^{WT}_EcoGPT	Takenoshita et al.[24]	N/A
pBS_Dsn1-N KI_GFP-Dsn1^{4A}_PuroR	This paper	N/A
pBS_Dsn1-N KI_GFP-Dsn1^{4A}_EcoGPT	This paper	N/A
pBS_Dsn1-N KI_GFP-Dsn1$^{\Delta 93–114}$_PuroR	This paper	N/A
pBS_Dsn1-N KI_GFP-Dsn1$^{\Delta 93–114}$_EcoGPT	This paper	N/A
pAID1.2-CMV-NmScarlet-mAID	Nishimura et al.[41]	Addgene plasmid #140618
pBS_PGK N-KI_ pCMV-OsTIR1-T2A-BSR-IRES-mScarlet-mAID-CENP-T	This paper	N/A
pBS_CENP-T N-KI_NeoR	Takenoshita et al.[24]	N/A
pBS_CENP-T N-KI_HisD	This paper	N/A
pBS_CENP-T N-KI_3xFLAG-CENP-T^{WT}_NeoR	Takenoshita et al.[24]	N/A
pBS_CENP-T N-KI_3xFLAG-CENP-T^{WT}_HisD	This paper	N/A
pBS_CENP-T N-KI_ 3xFLAG-CENP-T$^{\Delta 161–216}$_NeoR	This paper	N/A

(*Continued on next page*)

Continued

REAGENT or RESOURCE	SOURCE	IDENTIFIER
pBS_CENP-T N-KI_ 3xFLAG-CENP-T$^{\Delta 161–216}$_HisD	This paper	N/A
pBS_CENP-T N-KI_ 3xFLAG-CENP-T^{2A}_NeoR	This paper	N/A
pBS_CENP-T N-KI_ 3xFLAG-CENP-T^{2A}_HisD	This paper	N/A
Software and algorithms		
GraphPad Prism 9.5.1	GraphPad	https://www.graphpad.com/; RRID:SCR_002798
Fiji	Schindelin et al.[42]	https://imagej.net/ij/; RRID:SCR_002285
Image Lab 6.0.1	Bio-Rad	https://www.bio-rad.com/en-jp/product/image-lab-software?ID=KRE6P5E8Z; RRID:SCR_014210
Imaris 9.1.2	Bitplane	RRID:SCR_007370
Xcalibur4.6	Thermo Fisher	RRID:SCR_014593
Orbitrap eclipse tune application v.4.0.4091	Thermo Fisher	N/A

EXPERIMENTAL MODEL AND STUDY PARTICIPANT DETAILS

Cell culture

Chicken DT40 cells[38] were cultured in Dulbecco's modified Eagle's medium (Nacalai Tesque) containing 10% fetal bovine serum (Sigma), 1% chicken serum (Thermo Fisher Scientific), 10 μM 2-mercaptoethanol (Sigma), and penicillin (100 units/mL)-streptomycin (100 μg/mL) (Thermo Fisher Scientific) at 38.5°C with 5% CO_2. For degradation of mScarlet-mAID-CENP-T in AID based-CENP-T conditional knockdown cells, 500 μM 3-indole acetic acid (IAA; Wako) was added. All cell lines utilized in this study are listed in the key resources table. DT40 cells were tested for mycoplasma contamination.

METHOD DETAILS

Plasmid constructions

GFP-Dsn1^{WT}, GFP-Dsn1^{4A} (S97A, S101A, S102A, and S111A),[18] GFP-Dsn1$^{\Delta 93–114}$, and Dsn1^{WT}-spot were cloned into the plasmid containing approximately 2 kb homology arm around the start codon of *Dsn1* with the puromycin resistance gene cassette and EcoGPT gene cassette by In-Fusion® HD (TAKARA) (pBS_Dsn1-N KI_GFP-Dsn1^{WT}, _GFP-Dsn1^{4A}, _GFP-Dsn1$^{\Delta 93–114}$, or _Dsn1^{WT}-spot_PuroR or _EcoGPT).

cDNA for CENP-T full-length sequence was cloned into pAID1.2-CMV-NmScarlet-mAID (Addgene; #140618). To express the OsTIR1-T2A-BSR and mScarlet-mAID-CENP-T under control of the *CMV* promoter from the *PGK* locus, CMV promoter_OsTIR1-T2A-BSR_IRES_mScarlet-mAIDCENP-T fragment was cloned into the plasmid containing approximately 2 kb genome homology arm around the start codon of *PGK* by In-Fusion® HD (TAKARA) (pBS_PGK N-KI_pCMV-OsTIR1-T2A-BSR-IRES-mScarlet-mAID-CENP-T).

cDNA for CENP-T full-length sequence was cloned into p3xFLAG-CMV-10 (SIGMA). Several CENP-T mutants (CENP-T$^{\Delta 161–216}$, CENP-T^{RR-AA}, CENP-T$^{IFV-RRR}$, and CENP-T^{2A}) were generated by PCR based mutagenesis. These 3xFLAG-CENP-T mutants were then cloned into the plasmid containing approximately 2 kb homology arm around the start codon of *CENP-T* with the neomycin resistance gene cassette and hisD gene cassette by In-Fusion® HD (TAKARA) (pBS_CENP-T N-KI_3xFLAG-CENP-T^{WT}, _3xFLAG-CENP-T$^{\Delta 161–216}$, _3xFLAG-CENP-T^{RR-AA}, _3xFLAG-CENP-T$^{IFV-RRR}$, or _3xFLAG-CENP-T^{2A} _NeoR or _HisD).

Generation of cell lines

To express the GFP-Dsn1 constructs under control of the endogenous *Dsn1* promoter, pBS_Dsn1-N KI_GFP-Dsn1^{WT}, _GFP-Dsn1^{4A}, or _GFP-Dsn1$^{\Delta 93–114}$_PuroR and pBS_Dsn1-N KI_GFP-Dsn1^{WT}, _GFP-Dsn1^{4A}, or _GFP-Dsn1$^{\Delta 93–114}$_EcoGPT were transfected with pX330_ggDsn1[24] using Neon Transfection System (Thermo Fisher) with 6 times of pulse (1400 V, 5 msec) in CL18 (wild-type) cells, CENP-C$^{\Delta 73}$cells,[24] and CENP-C$^{\Delta 73}$ cells expressing mScarlet-mAID-CENP-T.

To express the Dsn1-spot constructs under control of the endogenous *Dsn1* promoter, pBS_Dsn1-N KI_Dsn1^{WT}-spot_PuroR and pBS_Dsn1-N KI_Dsn1^{WT}-spot_EcoGPT were transfected with pX330_ggDsn1-intron1 (GTAAGCGACGTTGTGGGCCG) using Neon Transfection System (Thermo Fisher) with 6 times of pulse (1400 V, 5 msec) in CENP-C$^{\Delta 73}$ cells expressing 3xFLAG-CENP-T.

To express OsTIR1-T2A-BSR_IRES_mScarlet-mAID-CENP-T construct under control of the CMV promoter from the endogenous *PGK* locus, pBS_PGK N-KI_pCMV-OsTIR1-T2A-BSR-IRES-mScarlet-mAID-CENP-T was transfected with pX335_ggPGK[40] using Neon Transfection System (Thermo Fisher) with 6 times of pulse (1400 V, 5 msec) in CENP-C$^{\Delta 73}$ cells.[24]

To express 3xFLAG-CENP-T constructs under control of the endogenous *CENP-T* promoter, pBS_CENP-T N-KI_3xFLAG-CENP-T^{WT}, 3xFLAG-CENP-T$^{\Delta 161–216}$, 3xFLAG-CENP-T^{RR-AA}, 3xFLAG-CENP-T$^{IFV-RRR}$, or 3xFLAG-CENP-T^{2A}_NeoR and pBS_CENP-T N-KI_3xFLAG-CENP-T^{WT}, 3xFLAG-CENP-T$^{\Delta 161–216}$, 3xFLAG-CENP-T^{RR-AA}, 3xFLAG-CENP-T$^{IFV-RRR}$, or 3xFLAG-CENP-T^{2A}_HisD

were transfected with pX330_ggCENP-T (TCCGAGAGGTCCGTCATGGA) using Neon Transfection System (Thermo Fisher) with 6 times of pulse (1400 V, 5 msec) in CENP-C$^{\Delta 73}$/GFP-Dsn1^{WT} cells expressing mScarlet-mAID-CENP-T, CENP-C$^{\Delta 73}$/GFP-Dsn1^{4A} cells expressing mScarlet-mAID-CENP-T.

The transfected cells were selected in the medium containing appropriate selection drugs (0.5 μg/mL puromycin (TAKARA) for the selection of PuroR expression, 25 μg/mL mycophenolic acid (Wako) and 125 μg/mL xanthine (SIGMA) for the selection of EcoGPT expression, 25 μg/mL Blasticidin S hydrochloride (Wako) for the selection of BSR expression, and L-histidinol for the selection of HisD expression) in 96 well plates to isolate single colonies.

Structure prediction

Structures were predicted with AlphaFold2-Multimer through ColabFold using MMseqs2 and default settings.[43] The structural figures were prepared using UCSF ChimeraX.

Immunoblot

DT40 cells were collected, washed with cold PBS, and suspended in 1xLaemmli Sample Buffer (LSB; 62.5 mM Tris-HCl (pH 6.8), 10 % Glycerol, 2% SDS, 5% 2-mercaptoethanol, bromophenol blue) (final concentration 1x10^4 cells/μL). Following the sonication, the lysate was heated at 96°C for 5 min.

The collected samples (1x10^5 cells) were separated by SDS-PAGE (SuperSep Ace, 5–20%; Wako) and transferred onto PVDF membranes (Immobilon®-P; Merck). The membrane was probed with primary antibody diluted with Signal Enhancer Hikari (Nacalai Tesque) at 4°C for overnight. After washing with 0.1% TBST (TBS, 0.1% Tween 20) for 15 min, the membrane was probed with secondary antibody diluted with Signal Enhancer Hikari (Nacalai Tesque) at room temperature for 1 h. After washing with 0.1% TBST for 15 min, the signals were detected using ECL Prime (GE Healthcare) and visualized by ChemiDoc Touch imaging system (Bio-Rad). The Image processing was performed using Image Lab 5.2.1 (Bio-Rad) and Photoshop CC (Adobe).

Primary antibodies used in immunoblot analyses were rabbit polyclonal anti-chicken CENP-T,[5] rabbit polyclonal anti-chicken CENP-C,[30] rabbit polyclonal anti-chicken Dsn1,[18] mouse monoclonal anti-FLAG M2 (Sigma), rat polyclonal anti-RFP (Chromotek), and mouse monoclonal anti-α-tubulin (Sigma). Secondary antibodies used in immunoblot analysis were horseradish peroxidase-conjugated (HRP)-conjugated goat polyclonal anti-rabbit IgG, HRP-conjugated goat polyclonal anti-Rat IgG, and HRP-conjugated rabbit polyclonal anti-mouse IgG (Jackson ImmunoResearch).

Immunoprecipitation

For 3xFLAG-CENP-T immunoprecipitation, cells expressing mScarlet-mAID-CENP-T and 3xFLAG-CENP-T were cultured with 500 μM IAA for 12 h and with 100 ng/mL nocodazole for the last 10h. These cells were collected, washed with cold PBS twice, suspended in Lysis buffer (20 mM Hepes-NaOH (pH 7.4), 150 mM NaCl, 0.1% NP40, 5 mM 2-mercaptoethanol, 1xcomplete EDTA-free proteinase inhibitor (Roche), and 1xPhosSTOP (SIGMA)) (final: 2x10^8 cells/mL) and sonicated. The lysate was treated with TURBO nuclease (50 unit/mL) for 30 min, clarified by centrifugation, and the supernatant was incubated with Protein-G Dynabeads (Thermo Fisher Scientific) conjugated to anti FLAG-M2 antibody at 4°C for 1 h. Proteins precipitated with anti-FLAG-M2 monoclonal antibody bound beads were washed with Lysis buffer three times, eluted with 2×LSB. The eluted samples were heated at 96°C for 5 min and subjected to immunoblot analysis.

Immunofluorescence analysis

The cells were cytospan onto slide glasses or coverslips by the Cytospin3 centrifuge (Shandon). For the CENP-T staining, cells were fixed with 3% paraformaldehyde (PFA) in 250 mM HEPES-NaOH (pH 7.4) at RT for 10 min and permeabilized in 0.5% NP-40 in PBS at RT for 10 min. For the CENP-A staining, cells were fixed with 3% paraformaldehyde (PFA) in 250 mM HEPES-NaOH (pH 7.4) at RT for 30 sec and fixed with methanol at -30°C for 20 min. After blocking with 0.5% BSA in PBS for 5 min, the cells were incubated with primary antibodies diluted in 0.5% BSA in PBS at 37°C for 1 h. The cells were washed three times with 0.5% BSA in PBS, incubated with secondary antibodies diluted in 0.5% BSA in PBS at 37°C for 1 h, and washed three times with 0.5% BSA in PBS. The cells were post-fixed for 10 min. DNA was stained with 100 ng/mL DAPI in PBS for 20 min. The stained cells were mounted with VECTASHIELD Mounting Medium (Vector Laboratories).

Primary antibodies used in immunofluorescence analysis were rabbit polyclonal anti-chicken CENP-T,[5] rabbit polyclonal anti-chicken CENP-A,[37] and mouse monoclonal anti-FLAG-M2 (Sigma). Secondary antibodies used in immunofluorescence analysis were Cy3-conjugated mouse polyclonal anti-rabbit IgG and Cy3-conjugated goat polyclonal anti-mouse IgG (Jackson ImmunoResearch).

Image acquisition

Immunofluorescence images were acquired every 0.2 μm intervals of z-slice using a Zyla 4.2 sCMOS camera (ANDOR) mounted on a Nikon Eclipse Ti inverted microscope with an objective lens (Nikon; Plan Apo lambda 100x/1.45 NA) with a spinning disk confocal scanner unit (CSU-W1; Yokogawa) controlled with NIS-elements (Nikon). The images in the figures are the maximum intensity projection of the Z-stack generated with Fiji.[42]

Chromosome alignment assay

The cells were treated with IAA (500 μM) for 12 h and incubated with MG132 (10 μM) for the last 2 h and harvested. The harvested cells were fixed and immunostained with anti-CENP-A antibody as above and mounted with VECTASHIELD Mounting Medium. The cells images were acquired by the confocal microscopy with spinning-disc. The chromosome alignment was analyzed according to a previous report.[44] Briefly, the XY positions of CENP-A signals in mitotic cells were acquired using the Imaris software and plotted on a two-dimensional plane. Scatter plot analysis was performed with confidence ellipses using Real Statistics in Excel (www.real-statistics.com). Chromosome alignment was assessed by calculating the ratio of the semi-major axis to the semi-minor axis of the ellipse and subtracting 1 to obtain the alignment value. As DT40 cells are maintained in a suspension culture, the data includes values from various angles, including non-side view chromosomes. However, since the experimental conditions are the same for all samples, comparing the control and experimental data appropriately provides us reliable data to evaluate the chromosome alignment. The experiments were repeated twice. Representative data of technical replicates are presented.

Flow cytometry analysis

The cell cycle distribution was analyzed according to a previous report.[45] The cells were treated with IAA (500 μM) for 12 h and incubated with 20 μM BrdU (5-bromo-2-deoxyuridine) for 20 min and harvested. The harvested cells were washed with the ice-cold PBS, fixed with 70% ethanol at –30°C. The fixed cells were washed with 1% BSA/PBS, incubated in 4 N HCl with 0.5% Triton X-100 at RT for 30 min, and washed with 1% BSA/PBS three times. The cells were incubated with an anti-BrdU antibody (BD, 347580) at RT for 1 h and washed with 1% BSA/PBS two times. Then, the cells were incubated with FITC-conjugated anti-mouse IgG (Jackson ImmunoResearch, 115-095-003; at 1:20 dilution in 1% BSA/PBS) at RT for 30 min, washed with 1% BSA/PBS and stained DNA with propidium iodide (10 μg/mL) in 1% BSA/PBS at 4°C overnight. The stained cells were applied to a Flow cytometry (BD; FACS Canto II). The cell cycle gates were manually adjusted based on plots of CENP-C$^{\Delta 73}$/CENP-T^{WT} cells, clearly distinguishing between subG1, G1, S, and G2/M populations, which were then applied to other cell lines. The percentages of each cell cycle stage (subG1, G1, S, G2/M phase or others cell) were calculated. The experiments were repeated twice. Representative data of technical replicates are presented.

LC-MS/MS analysis

For 3xFLAG-CENP-T immunoprecipitation, cells expressing 3xFLAG fused CENP-T, spot-fused Dsn1, and CENP-C$^{\Delta 73}$ were cultured with 100 ng/mL nocodazole for 12 h. These cells were collected, washed with cold PBS twice, and suspended in 300 μL Lysis buffer (20 mM Hepes-NaOH (pH 7.4), 150 mM NaCl, 0.1% NP40, 5 mM 2-mercaptoethanol, 1xcomplete EDTA-free proteinase inhibitor (Roche), and 1xPhosSTOP (SIGMA) (final: 2x10^8 cells/mL)). The suspension was then sonicated. The lysate was treated with TURBO nuclease (50 units/mL) for 30 min, clarified by centrifugation, and the supernatant was incubated with Protein-G Dynabeads (Thermo Fisher Scientific) conjugated to anti FLAG-M2 antibody at 4°C for 2 h. Proteins precipitated with anti FLAG-M2 antibody-bound beads were washed with 30 μL Lysis buffer five times and eluted with 25 μL Elution buffer (150 μg/mL 3xFLAG-peptide in Lysis buffer) four times.

For LC-MS/MS analysis, eluted samples underwent reduction with 10 mM Tris(2-carboxyethyl)phosphine Hydrochloride (TCEP) and alkylation via incubation with 55 mM iodoacetamide (IAA) for 30 min at room temperature in the dark. Trypsin digestion and sample cleanup were performed using the SP3 method.[46]

Mass spectra were acquired with an Orbitrap Eclipse (Thermo Fisher Scientific) coupled to a nanoflow UHPLC system (Vanquish; Thermo Fisher Scientific). The peptide mixtures were loaded onto a C18 trap column (PepMap Neo Trap Cartridge, ID 0.3 mm x 5 mm, particle size 5 μm, Thermo Fisher Scientific) and fractionated through the C18 analytical column (Aurora, ID 0.075 × 250 mm, particle size 1.7 μm, IonOpticks). The peptides were eluted at a flow rate of 300 nL/min using the following gradient: 0% to 2% solvent B over 1 minute, 2% to 5% over 2 minutes, 5% to 16% over 19.5 minutes, 16% to 25% over 10 minutes, 25% to 35% over 4.5 minutes, a sharp increase to 95% over 4 minutes, hold at 95% for 5 minutes, and finally re-equilibration at 5%. Solvent A and B compositions were 100% H2O, 0.1% Formic acid and 100% Acetonitrile, 0.1% Formic acid, respectively. The Orbitrap operated in a data-dependent mode with a 3-second cycle time. The MS1 scan was collected at 60,000 resolution, the mass range 375 -1500 m/z, using a standard AGC and maximum injection time of 50 ms. MS/MS was triggered from precursors with intensity above 20,000 and charge states 2-7. Quadrupole isolation width was 1.6 m/z, with normalized HCD energy of 30%, and resulting fragment ions recorded in Orbitrap. MS1 scan was collected at 15,000 resolution with standard AGC target and maximum injection time of 22 ms. Dynamic exclusion was set to 20 seconds.

The raw data files were searched against the Gallus gallus dataset (Uniprot Proteome UP000000539, downloaded on 20230703) with the common Repository of Adventitious Proteins (cRAP, ftp://ftp.thegpm.org/fasta/cRAP) and 3xFlag sequence for contaminant protein identification, using Proteome Discoverer 2.5 software (Thermo Fisher Scientific) with MASCOT ver.2.8 search engine, with a false discovery rate (FDR) set at 0.01. The number of missed cleavages sites was set as 2. Carbamidomethylation of cysteine was set as a fixed modification. Oxidation of methionine, phosphorylation of serine, threonine and tyrosine, and acetylation of protein N-termini were set as variable modifications.

Nocodazole sensitivity assay

The cells were treated with IAA (500 μM) for 12 h. The IAA treated-cells (1x10^5 cells/mL) were then treated with nocodazole at indicated concentrations (5, 10, 15, or 20 ng/mL) for 24 h. After nocodazole treatment, 100 μL of cells were seeded onto opaque-walled tissue culture 96 well plates with a clear bottom. 20 μL of RealTime-Glo reagents premix (1/10000 substrate and 1/10000 enzyme in DMEM; RealTime-Glo MT Cell Viability Assay; Promega) were added to the cells and incubated for 1 h at 37°C. Luminescence signal was measured using a GloMax Discover System Microplate Reader (Promega). IC50 was calculated using GraphPad Prism by fitting the data to a sigmoidal dose-response curve with a 4 parameter logistic (4PL) model, where the X-axis represents the logarithm of the concentration. The experiments were repeated three times, and the mean and standard deviation (SD) are shown.

QUANTIFICATION AND STATISTICAL ANALYSIS

The fluorescence signal intensities of GFP-Dsn1 at more than 80 kinetochores in each of 10 cells and background signals in non-kinetochore region for each sample were quantified using the Imaris software (Bitplane). The mean fluorescence signal intensities at kinetochores in each cell were subtracted by the mean background signal intensity in the non-kinetochore region. Each experiment was repeated two (Figure 1E) or three times (Figures 3C, 3G, 4E, 5D, and 6B). Representative data of technical replicates are presented. Statistical analyses were performed using GraphPad Prism (GraphPad Software).